Contributions to Mineralogy and Petrology (2021) 176:63
https://doi.org/10.1007/s00410-021-01814-4

ORIGINAL PAPER

Ferrous/ferric (Fe^{2+}/Fe^{3+}) partitioning among silicates in metapelites

Jacob B. Forshaw[1] · **David R. M. Pattison**[1]

Received: 8 March 2021 / Accepted: 30 June 2021

Abstract

Fe^{3+} and X_{Fe3+}, defined as $Fe^{3+}/(Fe^{2+}+Fe^{3+})$ on a molar basis, are now recognised as key parameters in phase equilibrium modelling. A hindrance is that it is only possible to routinely measure total Fe, and not Fe^{3+} and Fe^{2+}, in minerals using the electron microprobe. Charge balance techniques can be used to estimate Fe^{3+} and Fe^{2+} for some minerals, but not for those that contain vacancies. Whilst other analytical techniques can determine X_{Fe3+} in minerals, these are not commonly applied by metamorphic petrologists. Therefore, researchers must rely on estimates. This study collates wet chemical, Mössbauer spectroscopy, and X-ray absorption near edge structure (XANES) spectroscopy analyses of X_{Fe3+} in metapelitic minerals and rocks from the literature. The resulting database of 77 studies contains 591 samples, of which 261 have X_{Fe3+} determined for the whole rock. There are X_{Fe3+} measurements for 483 biotites, 192 white micas, 78 chlorites, and 32 staurolites. Average ($\pm 1\sigma$) X_{Fe3+} values in whole rock, biotite, white mica, chlorite, and staurolite are 0.23 ± 0.16, 0.11 ± 0.08, 0.55 ± 0.18, 0.08 ± 0.07, and 0.07 ± 0.06, respectively. The average ($\pm 1\sigma$) number of Fe^{3+} cations in biotite, white mica, chlorite, and staurolite is 0.28 ± 0.19 (22 O + Ti cations per formula unit, pfu), 0.17 ± 0.13 (22 O pfu), 0.31 ± 0.27 (28 O pfu), and 0.20 ± 0.17 (46 O pfu), respectively. The mean whole rock X_{Fe3+} is similar for metapelites containing ilmenite and magnetite, as well as those that report no Fe-oxide, but is considerably higher for hematite-bearing rocks. Whilst there is little variation with pressure and temperature, there is an increase in the number of Fe^{3+} cations and X_{Fe3+} of both white mica and biotite with the type of Fe-oxide present. Our observations are compared with the predictions of phase equilibrium modelling using thermodynamic dataset 6.2 (Holland and Powell, J Metamorph Geol 29:333–383, 2011) and the solution models of White et al. (J Metamorph Geol 32:261–286, 2014a) for Fe^{3+} and X_{Fe3+} in these minerals. The predicted X_{Fe3+} and number of Fe^{3+} cations in biotite, chlorite, and staurolite broadly match natural observations, but for white mica the predicted mean X_{Fe3+} is underestimated by 0.2–0.4 and the number of Fe^{3+} cations by 0.05–0.2. Whilst modelling correctly predicted increases in the X_{Fe3+} of white mica and biotite with whole rock X_{Fe3+}, it also predicted variations in mineral X_{Fe3+} as a function of pressure and temperature which are not observed in the natural samples.

Keywords Ferrous/ferric · Fe^{2+}/Fe^{3+} · X_{Fe3+} · Metapelites · Wet chemical · Oxidation state

Introduction

Since the advent of the electron probe micro-analyser (EPMA) as an analytical tool for geologists, major element geochemical characterisation of minerals has become routine. However, routine EPMA analysis can only determine total Fe, not Fe oxidation states (Fe^{2+} and Fe^{3+}). This has long been recognised as a problem for metamorphic petrologists. For example, Fe–Mg thermometry is based on the exchange of Fe^{2+} and Mg, not total Fe, yet several minerals contain enough Fe^{3+} to affect the Fe/Mg ratio and thus the temperature estimate (Guidotti and Dyar 1991; Holdaway et al. 1997; Schumacher 1991). As a result, authors have attempted to determine Fe^{3+} from EPMA data using recalculation schemes based on charge balancing (Droop 1987), or a procedure known as the Flank Method (Höfer et al. 1994). These techniques are mainly applicable to anhydrous silicates and oxides (e.g., garnet, pyroxene, spinel, and Fe-oxides). Whilst empirical estimates of ferric iron contents have been developed for some hydrous minerals, (e.g., amphibole; Hawthorne et al. 2012; Holland and Blundy

Communicated by Daniela Rubatto.

✉ Jacob B. Forshaw
jacob.forshaw1@ucalgary.ca

[1] Department of Geoscience, University of Calgary, 2500 University Drive NW, Calgary, AB T2N 1N4, Canada

Published online: 09 August 2021

1994; Robinson et al. 1982; Schumacher 1991, 2007; Stout 1972), the same cannot be done for minerals that contain more than one partially filled site such as biotite, white mica, chlorite, and staurolite (Schumacher 1991). Li et al. (2019) attempted to expand the Flank Method for use in biotite, but this approach is not widely used and requires further testing. Whilst other analytical techniques, such as Mössbauer spectroscopy, electron energy-loss spectroscopy (EELS), X-ray photoelectron spectroscopy (XPS), and X-ray absorption near edge structure (XANES) spectroscopy at the K edge have been used to determine Fe^{3+} in minerals, they have only been applied in a relatively small number of studies. Therefore, when considering Fe^{3+}, researchers must rely on estimates of Fe^{3+} in several rock-forming minerals.

Before the widespread use of EPMA, authors painstakingly separated minerals from rocks and used wet chemical techniques to determine their compositions, including Fe^{2+} and Fe^{3+}. Several compilations of wet chemical data exist in the literature from studies concerned with crystal–chemical classifications of individual silicates (e.g., Foster 1960, 1962, 1964); however, these works generally collated analyses from a wide variety of rock types (felsic to mafic igneous and/or metamorphic) and most only considered Fe^{3+} contents in a single mineral from each sample. This study focuses on the ferrous/ferric ratios of silicates in metamorphosed siliciclastic rocks (e.g., pelites and semi-pelites), which are widespread in the rock record and widely used as indicators of metamorphic grade. Only one extensive study to date has measured Fe^{2+} and Fe^{3+} in multiple metapelitic minerals from individual rocks (Dyar 1990; Dyar et al. 1991, 2002; Guidotti et al. 1994; Guidotti and Dyar 1991). These authors examined the Fe^{3+} contents of different minerals from across a regional, medium-pressure metamorphic sequence (garnet–staurolite–sillimanite–K–feldspar) in West-central Maine using both XANES and Mössbauer spectroscopy. Whilst the samples from Maine encompass a range of metamorphic grade, they equilibrated at approximately the same pressure and represent a narrow range of bulk compositions. Therefore, it may not be appropriate to use the Maine dataset as the basis for estimates of Fe^{3+} contents in other metapelites that equilibrated at different pressure–temperature (P–T) conditions and oxidation states.

Here, we have collated a database of Fe^{3+} contents in minerals from studies that analysed Fe^{2+} and Fe^{3+} using wet chemistry, Mössbauer spectroscopy, and XANES spectroscopy. The emphasis is on the metapelitic minerals biotite, white mica, chlorite, and staurolite because Fe^{3+} in these minerals cannot be estimated from EPMA data. We examine variation in the number of Fe^{3+} cations and X_{Fe3+} in these minerals as a function of metamorphic grade, pressure, and oxidation state using the type of Fe-oxide present in the rock as a proxy. We compare these observations with the predictions of phase equilibrium modelling using the Holland and Powell (2011) thermodynamic dataset 6.2 and White et al. (2014a) solution models.

Methods

Data selection and extraction

Papers and theses containing measurements of Fe^{2+} and Fe^{3+} in minerals were discovered through a series of Google Scholar and ProQuest searches using combinations of the following key words: ferrous, ferric, Fe^{3+}, wet chemical, metapelitic, metasedimentary, and metamorphism. Some searches were restricted to the date range 1955–1975 to filter out the many EPMA-based studies of later years which lack measurements of Fe^{3+}. To ensure we captured as many data as possible, manual searches through online archives between the years of 1955 and 1975 were conducted for the following journals: American Mineralogist, Bulletin de la Société Géologique de France, Contributions to Mineralogy and Petrology, Journal of the Faculty of Science University of Tokyo, Journal of the Geological Society of Japan, Journal of Petrology, Neues Jahrbuch für Mineralogie—Abhandlungen, Neues Jahrbuch für Mineralogie—Monatshefte, and Schweizerische Mineralogische und Petrographische Mitteilungen. Whilst it is inevitable that some data have eluded our searches, the resultant database is still substantial.

Three main criteria had to be met for a sample to be included in the database: (a) a measurement of Fe^{2+} and Fe^{3+} in one or more of white mica (e.g., muscovite, phengite, sericite), biotite, chlorite, and staurolite; (b) a list of the major minerals in the assemblage; and (c) a description indicating that the sample was a metamorphosed siliciclastic rock (e.g., mudstone/siltstone/immature sandstone protolith; pelite/semi-pelite). Since the majority of samples included in the database are metapelites, we use this term throughout the rest of the paper to describe the samples; however, the reader should note that a small subset of the samples would be strictly classified as semi-pelites or metagreywackes.

Some studies also presented analyses of garnet, cordierite, and chloritoid in the same selected samples; however, these have not been included in the database for the following reasons: measurements of Fe^{3+} in garnet and cordierite from pelites and semi-pelites indicate that there is negligible Fe^{3+} in them (e.g., Dyar et al. 2002, 2012; unpublished; Geiger et al. 2000a, b; Williams and Grambling 1990); Fe^{3+} in garnet and chloritoid can be estimated from EPMA data using a charge-balancing approach (Droop 1987); and there are relatively few Fe^{3+} analyses of cordierite and chloritoid in the literature.

For analyses of minerals and rocks, the weight per cent oxides for all elements (not just FeO and Fe_2O_3) were taken from the original sources. In some cases, only the cations

per formula unit (e.g., Dyar et al. 1991), or the reported ratio of Fe^{3+} to total iron for each mineral (e.g., Dyar et al. 2002) were available.

Mineral formulae recalculation

Mineral formulae were recalculated from the original weight per cent oxides wherever possible. Cations could not be determined for partial analyses (e.g., Albee 1965; Card 1964; Chinner 1960; Goossens 1970). Using a fixed number of OH^- anions to calculate mineral formulae for phyllosilicates can be problematic since hydrogen contents may be non-stoichiometric (Dyar et al. 1993a). If the H_2O content of the mineral was measured then this problem could be negated, since normalisation could be based on the measured number of O/OH atoms per formula unit (pfu). However, only a few authors included H_2O contents in their analyses and most of these studies did not indicate whether H_2O contents were measured or estimated. To be consistent in our recalculations, we did not incorporate stated H_2O contents. Careful consideration was therefore needed when deciding on the number of negative charges, using O^{2-} as the effective anion, in formula recalculation for biotite, white mica, and chlorite analyses.

Eugster and Wones (1962) first noted a correlation between the number of Fe^{3+} cations and the OH^- content of biotite. Since then, numerous workers have investigated how tetra- and tri-valent cations (e.g., Fe^{3+}, Ti^{4+}, Al^{3+}, Cr^{3+}, etc.) may be incorporated in the octahedral site of phyllosilicates through the loss of H^+ from the OH groups. This process is known by several names including: "oxy-substitution", "dehydrogenation", and "deprotonation". Foster (1964) found a low degree of correlation between Fe^{3+} and excess O in micas and chlorite, suggesting that whilst deprotonation may account for the excess charge in some samples, it did not in others. She concluded that Fe^{3+} contents are mainly determined by the redox state of the rock, as has been found in several subsequent studies (e.g., Dodge et al. 1969; Guidotti et al. 1994; Guidotti and Dyar 1991; Redhammer et al. 1993; Wones and Eugster 1965). Dyar et al. (1993a) demonstrated that in biotite, muscovite, and chlorite, deprotonation involving only the exchange of H^+ and Fe^{3+} is rare and is better considered as an exchange involving all tetra- and tri-valent cations in a mineral. Cesare et al. (2003) concluded that Ti^{4+} accounts for the majority of the H deficiency in biotite from metapelitic samples, in agreement with the observations of Righter et al. (2002) and Waters and Charnley (2002). Since our study focusses on metapelitic rocks, we accept the findings of these studies and have therefore determined our biotite formulae based on a 22 O + Ti cations recalculation.

Concerning muscovite, deprotonation is thought to be minor (Dyar et al. 1993a; Guidotti and Sassi 1998a, b), whereas for chlorite, some have postulated that deprotonation may aid incorporation of Fe^{3+} in the octahedral site (Lempart et al. 2018, 2020; Masci et al. 2019; Walshe 1986). We have found no well-documented studies of the H^+ and Fe^{3+} contents of chlorite or muscovite in metapelitic rocks. Therefore, we have recalculated muscovite and chlorite analyses using a fixed number of anions: 22 and 28 O pfu, respectively. Staurolite analyses were recalculated using 46 O pfu (Deer et al. 2013). The number of oxygens per formula unit chosen for each mineral here is the same as in the White et al. (2014a) solution models, which maintains consistency between our natural data and thermodynamic predictions to be discussed below.

Two important parameters related to variations in Fe^{2+} and Fe^{3+} are X_{Fe3+} and X_{Mg}. These are defined on a molar basis as follows:

$$X_{Fe3+} = \frac{2Fe_2O_3}{2Fe_2O_3 + FeO} = \frac{Fe^{3+}}{Fe^{3+} + Fe^{2+}} \quad \text{(molar)},$$

$$X_{Mg} = \frac{MgO}{MgO + FeO} = \frac{Mg^{2+}}{Mg^{2+} + Fe^{2+}} \quad \text{(molar)}.$$

X_{Mg} is the ratio of Mg^{2+} to $(Mg^{2+} + Fe^{2+})$, not Mg^{2+} to $(Mg^{2+} + Fe^{total})$ as is commonly assumed in microprobe analyses that do not distinguish between Fe^{2+} and Fe^{3+}. Note that the above definition of X_{Fe3+} is equivalent to the oxidation ratio of Chinner (1960) divided by 100.

Analytical techniques

Measurements of Fe^{3+} in metapelitic rocks and minerals in our database were determined by wet chemistry, Mössbauer spectroscopy, or XANES spectroscopy. We briefly summarise these methods and refer the reader to the original studies for detailed descriptions. In the majority of wet chemical studies, Fe^{3+} was determined using a two-step dissolution process (see Fritz and Popp 1985 for a review). One portion of the sample is either completely oxidised, so that total iron can be measured as Fe_2O_3 by atomic absorption spectrophotometry, or alternatively completely reduced, so that total iron can be measured as FeO by colorimetry. A separate portion of the sample is dissolved without oxidation or reduction, in order to measure the sample's original FeO content using titration or colorimetry. The difference between the two values provides the amount of Fe^{3+} in the sample. Comparatively, XANES and Mössbauer spectroscopy measurements can only determine X_{Fe3+} (Bajt et al. 1994) and therefore must be combined with an EPMA analysis of Fe in order to quantify Fe^{3+}. Note that XANES spectroscopy is a microbeam technique that analyses X_{Fe3+} in-situ, whereas Mössbauer spectroscopy is similar to wet chemistry, in that it requires the sample to be crushed and

the mineral of interest separated so that it may be analysed in bulk. As a result, XANES measurements have sometimes found a wide range of Fe^{3+} contents at the scale of a thin section (e.g., Delaney et al. 1998; Dyar et al. 2002; Masci et al. 2019), which would not be detected in either Mössbauer spectroscopy or wet chemical analyses.

Database analysis

When compiling a database of this nature, there is inherent uncertainty and bias from several sources. First, we filtered the data by applying some quality controls (described below) to remove poor analyses. Second, we explored whether it is appropriate to pool analyses completed in different laboratories using a range of analytical techniques. Finally, we examined whether there is any bias in the database towards certain minerals, P–T conditions, or oxidation states.

Data filtering

It is not possible to independently verify that the values for individual elemental oxides (e.g., Fe_2O_3 and FeO) in analyses from literature studies are "good". However, we can assess the overall stoichiometry of an analysis in samples for which a complete chemical analysis was provided.

In micas we scrutinised the total number of octahedral and interlayer site cations per formula unit (Fig. 1). Micas with a full interlayer site have 2.0 cations (Ca, Na, and K); values greater than 2.0 or less than 1.6 are considered suspect, the lower value sometimes arising from inter-layer chlorite. To be conservative, we therefore only included analyses with total interlayer cations between 1.4 and 2.2 (Fig. 1). White micas are dominantly dioctahedral with 4.0 cations in the octahedral site, whilst biotites are dominantly trioctahedral with 6.0 cations in the octahedral site. Some solid solution is possible, meaning that values between 4.0 and 6.0 cations are plausible (c.f. Tischendorf et al. 2007). Values outside 4.0–6.0 are unlikely, and where measured suggest some contamination. Being conservative, we only included analyses with total octahedral cations between 3.8 and 6.2 (Fig. 1). In chlorite the total number of cations per formula unit ranges from 8.0 (di-dioctahedral) to 10.0 (tri-trioctahedral), therefore to be conservative, we only included analyses with total cation sums between 7.8 to 10.2 (c.f. Zane and Weiss 1998). In staurolite, the total number of cations per formula unit is typically between 29.0 and 30.0, therefore, we only included analyses with total cation sums of 28.8–30.2 (c.f. Hawthorne et al. 1993).

The resulting database of 77 studies contains 591 samples from 47 localities, the latter listed in Table 1. Online Resource 1 (Table S1) details the full database of samples including name, metamorphic zone, assemblage, minerals analysed, and whether whole rock data are available. 261 samples (44.2%) were analysed for whole rock X_{Fe3+} (Online Resource 1—Table S2). There are 785 individual minerals with measured X_{Fe3+} including 483 biotites, 192 white micas, 78 chlorites, and 32 staurolites (Online Resource 1—Tables S3–6). After omitting partial analyses, the number of Fe^{3+} cations could be calculated for 456 biotites, 190 white micas, 60 chlorites, and 26 staurolites.

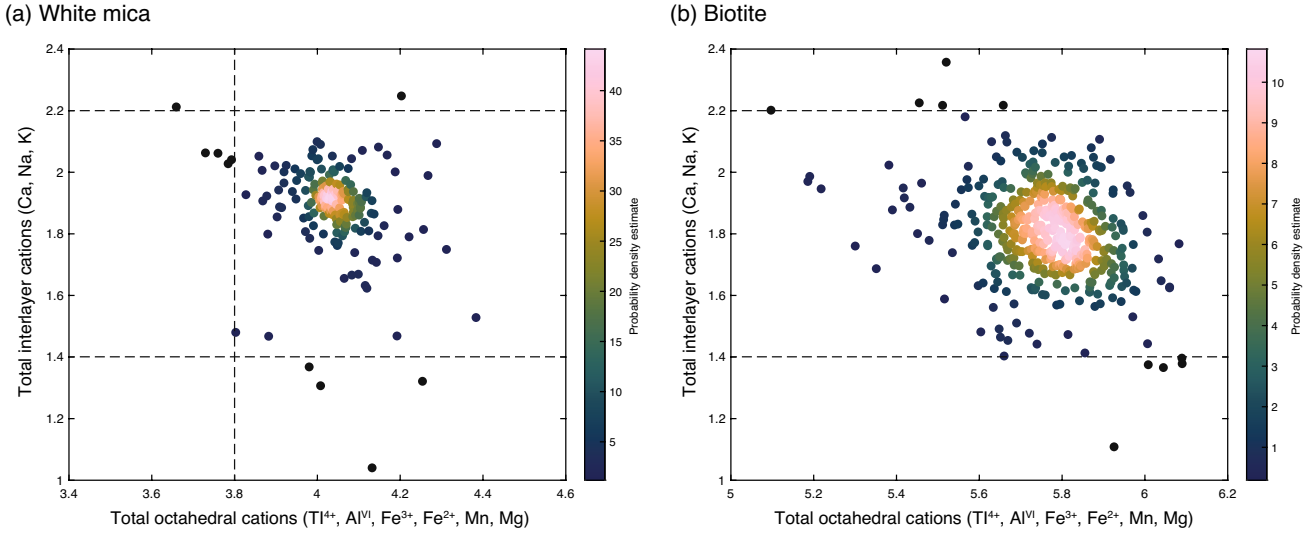

Fig. 1 Total interlayer site cations vs. total octahedral site cations for **a** white mica (22 O pfu) and **b** biotite (22 O + Ti cations pfu). Colour bars show the 2D probability density estimate for the data. Grey dots represent analyses which were removed. Dashed lines show the stoichiometric constraints used to filter analyses

Table 1 Geographic and/or geologic locations of regions with ferrous/ferric data for silicate minerals, listed alphabetically

Locality	Country	#S	#A	Facies	References
Agnew Lake	Canada	5	5	A	Card (1964)
Albany	Australia	17	34	UA–GR	Stephenson (1979)
Alpine	Switzerland /Italy	39	79	A	Goossens (1970), Hansen (1972), Hunziker (1966), Schwander et al. (1968), Wenk et al. (1963), Wetzel (1973)
Beawar	India	9	21	A	Sharma and Narayan (1975a, b)
Blue Ridge	USA	19	27	UA–GR	Eckert (1988), Mohr and Newton (1983)
Connemara	Ireland	1	3	A	Leake (1958)
Dalradian	Scotland	51	106	GS–A–GR	Atherton (1968), Chinner (1960, 1962, 1965), Mather (1970), McNamara (1965), Snelling (1957)
Darjeeling	India	3	3	A	Chakraborty and Sen (1967), Sen and Chakraborty (1968)
Davis Creek	New Zealand	2	4	UA	Hattori (1967)
Dill	Canada	13	31	A	Kwak (1968)
Dutchess	USA	24	48	UA	McKay (1964)
Egremont	USA	3	8	A	Zen (1981)
El Hoyazo	Spain	4	4	UA–GR	Cesare et al. (2003, 2005)
Errol	USA	3	3	A	Dyar et al. (1991), Green (1963)
Fichtelgebirge	Germany	20	41	GS–A	Mielke et al. (1979)
Flinton	Canada	8	16	A	Hounslow and Moore (1967)
Guri	Venezuela	10	20	UA–GR	Dougan (1974)
Harcourt	Canada	4	5	UA–GR	Lal and Moorhouse (1969)
Hunt Valley	USA	4	4	A	Dyar et al. (1991)
Kandra	India	7	14	A	Chakraborty and Sen (1967), Sen and Chakraborty (1968)
Khetri	India	4	8	A	Lal and Shukla (1975)
Kumaon	India	7	20	GS–A	Das (1973)
Lincoln	USA	12	16	A	Albee (1965)
Littleton	USA	8	9	A	Dyar et al. (1991), Lyons and Morse (1970), Shaw (1956)
Mt. Lofty	Australia	9	18	A	Fleming (1971, 1972)
Moine	Scotland	35	86	GS–A	Butler (1965,1967), Lambert (1959)
New South Wales	Australia	4	8	GS–A	Vallance (1960)
Old Saybrook	USA	3	5	A	Lundgren (1966)
Onawa	USA	12	12	A	Moore (1960)
Orange	USA	8	8	A	Hall (1970)
Otter Lake	Canada	4	4	UA–GR	Kretz (1990)
St. Paul Island	Canada	24	25	A	Phinney (1963)
Reading Prong	USA	3	3	UA–GR	Dallmeyer (1974)
Ryoke/Abukuma	Japan	33	50	A	Hayama (1964), Kutsukake (1976, 1977), Miyashiro (1956, 1958), Ono (1969)
Sambagawa	Japan	6	12	GS-A	Banno (1964)
Shetland	UK	2	4	GS–A	Flinn (1967)
Sierra Nevada	USA	6	6	A	Best and Weiss (1964)
Snow Peak	USA	6	17	A	Hietanen (1969)
Southern Alps	New Zealand	5	7	GS–A	Mason (1962)
Sparrow Lake	Canada	4	7	A	Kamineni (1975)
Steinach	Germany	8	20	A	Okrusch (1969, 1971)
Sturbridge	USA	1	2	UA–GR	Barker (1962)
Trondheim	Norway	10	17	GS	Saxena (1966)
Truchas	USA	11	11	A	Dyar et al. (1991), Williams and Grambling (1990)
West-central Maine	USA	86	137	A–G	Dyar (1990, unpublished), Dyar et al. (1991, 2002), Guidotti et al. (1994), Guidotti and Dyar (1991), Holdaway et al. (1997), Moeller (1991)
Westport	Canada	34	58	UA–GR	Blackburn (1967), Reinhardt (1968), Wynne-Edwards and Hay (1963)

#S = Number of samples included in database. #A = Number of analyses of X_{Fe3+} in rocks and minerals

GS greenschist, *A* amphibolite, *UA* upper amphibolite, *GR* granulite

Comparison of analytical techniques

For the 785 mineral X_{Fe3+} values in our database, 83.4% were measured using wet chemical methods, 12.5% via Mössbauer spectroscopy, and 4.2% by XANES. All whole rock X_{Fe3+} values in the database were determined by wet chemical methods. For the mineral analyses, an important question is whether different analytical techniques produce comparable measurements of Fe^{3+}. Only a small number of the minerals in the database were analysed using multiple techniques (4.1%). Williams and Grambling (1990) examined their biotite separates using both Mössbauer spectroscopy and wet chemical methods (six analyses; 0.8% of the database); they found that the techniques gave similar results, except in cases where there were local patches of alteration or fine mineral inclusions in biotite. Ten of the biotites studied using Mössbauer spectroscopy in Dyar (1990) were later analysed using XANES and wet chemical techniques by Delaney et al. (1998), who found that results of all three compared well with each other. Following this work, Dyar et al. (2002) published XANES analyses of biotite, muscovite, and chlorite, for which X_{Fe3+} had previously been determined using Mössbauer spectroscopy (3.3% of the database; Dyar 1990, unpublished; Guidotti et al. 1994; Guidotti and Dyar 1991; Moeller 1991). They found good agreement between the two techniques in all minerals except muscovite, for which the Mössbauer spectra typically showed lower values than XANES, especially at lower metamorphic grade; these authors interpreted this discrepancy as being due to contamination of the muscovite separates analysed by Mössbauer spectroscopy by fine-grained chlorite. We therefore replaced the values of X_{Fe3+} determined from the earlier Mössbauer studies with the X_{Fe3+} values determined by XANES.

Due to the relatively small number of samples in our metapelite database for which analyses were performed using more than one technique, we also examined studies in the literature from other rock types that employed multiple techniques. These studies were from igneous rocks or metamorphic rocks of a non-sedimentary nature, so the analyses were not included in our database. Several studies found good agreement between wet chemical and Mössbauer analyses in a range of minerals including micas, amphiboles, garnets, and pyroxenes (Bancroft and Brown 1975; Dodge et al. 1969; Dyar et al. 1993a, b; Dyar and Burns 1986; Ernst and Wai 1970; Fritz and Popp 1985; Lalonde et al. 1998; Whipple 1974; Williams and Grambling 1990). Lalonde et al. (1998) conducted a study of biotite that compared Mössbauer spectroscopy to the most common wet chemical methods in use. They found that results from the Pratt (1894) wet chemical method matched the results of Mössbauer spectroscopy better than the wet chemical results from the Wilson (1955,1960) method. Unfortunately, for the analyses in our database determined by wet chemistry, many authors did not provide detailed methods for how Fe^{2+} and Fe^{3+} were measured using wet chemistry, meaning we were unable to assess possible discrepancies arising from different techniques. For those authors that did fully detail their methods, they typically followed those outlined by Shapiro and Brannock (1956), which is similar to that of Pratt (1894).

Previous studies have also demonstrated a good agreement between Mössbauer and XANES data for several minerals including biotite, chlorite, staurolite, amphibole, olivine, pyroxene, and garnet (Delaney et al. 1996, 1998; Dyar et al. 2001, 2002; Evans et al. 2014; Righter et al. 2002). As noted above, one difference in the results of the two techniques is that in-situ XANES measurements have sometimes found a wide range of Fe^{3+} contents at the scale of a thin section (e.g., Delaney et al. 1998; Dyar et al. 2002; Masci et al. 2019). As a result, we have opted to only include XANES data from Dyar et al. (2002), where it showed good agreement with previous Mössbauer measurements.

In addition to measurements of Fe^{3+} and X_{Fe3+}, mineral analyses in the database include other elements (SiO_2, Al_2O_3, MgO, etc.) that were determined using either EPMA or wet chemistry. Although these analyses are not the focus of this paper, we note that many of the studies included in the database found good agreement between EPMA and wet chemical measurements of major elements in the same mineral (e.g., Fleming 1971; Hietanen 1969; Kretz 1990; Kwak 1968; Mielke et al. 1979; Okrusch 1969, 1971; Stephenson 1979; Zen 1981).

Number of analyses per mineral

Here we examine the number of analyses of each mineral included in the database. First, we calculate an *analysis percentage*, which is the number of times a mineral's X_{Fe3+} was analysed as a percentage of the number of times it was reported in an assemblage. Biotite has the most analyses of any mineral (483), and the greatest *analysis percentage* (90.3%). This is a result of its stability over a wide range of P–T space, its typically high mode in metapelites allowing for easy separation during crushing, and its role in geothermometry. White mica is the second most analysed mineral (192, 42.3%), followed by chlorite (78, 57.4%) and staurolite (32, 21.6%). Chlorite and staurolite have more restricted stability ranges than white mica and biotite, and staurolite may be difficult to analyse due to its commonly inclusion-rich nature.

Data classification with respect to pressure, temperature, and oxidation state

Here we consider any bias in the database towards rocks of certain pressures, temperatures, or oxidation states. Due to the different methods used to estimate P–T conditions in the original studies, we have opted for a mineral assemblage-based approach, in which samples have been categorised based on the metamorphic zone (temperature), prograde mineral assemblage sequence or "facies series" (pressure), and the type of Fe-oxide present (oxidation state). The rationale for each of these is given below and the categories are summarised in Fig. 2. The metamorphic zone, facies series, and type of Fe-oxide present for each sample is included in the overview summary of the database in Online Resource 1 (Table S1). Abbreviations for minerals follow Whitney and Evans (2010).

Temperature conditions were delineated based on five metamorphic zones found in metapelites: Chl/Bt, Grt, Crd/And/St/Ky (minerals whose initial development occurs at different pressures but similar temperature), Sil, and Kfs (Fig. 2). The Chl/Bt zone spans the greenschist facies of metabasic rocks, whilst the Grt, Crd/And/St/Ky, and Sil zones encompass the amphibolite facies. The Kfs zone covers the upper amphibolite–granulite facies transition. These zones are depicted on diagrams by the colour red, with progressively darker shades indicating higher grades (Fig. 2).

The pressure of metamorphism was distinguished based on five pressure-dependent prograde mineral assemblage sequences or "facies series" (Hietanen 1967; Miyashiro 1961): Crd-And-Sil (low-P Buchan), St-And-Sil (high-P Buchan), St–Ky–Sil (Barrovian), polymetamorphic, and unspecified (Fig. 2). The first three of these classifications represent broader, more inclusive versions of the facies series of Pattison and Tracy (1991); the Crd-And-Sil group incorporates facies series types 1a–2a, the St-And-Sil category includes types 2b-3, and the St–Ky–Sil group comprises type 4. Polymetamorphic rocks include those with three aluminosilicates reported by the authors (e.g., Williams and Grambling 1990) and those where contact metamorphism overprints regionally metamorphosed rocks (e.g., Chinner 1962; Okrusch 1969, 1971). Unspecified rocks comprise those of the greenschist or granulite facies that could not be linked to a facies series up- or down-grade, such as granulite facies xenoliths from El Hoyazo (Cesare et al. 2003, 2005). These pressure-dependent facies series are depicted on diagrams by the colour blue, with progressively darker shades indicating higher pressures (Fig. 2).

Concerning oxidation state, there are a number of ways that this parameter can be defined. One is to use the measurement of X_{Fe3+} in the whole rock, however, this would neglect 55.8% of the samples. Therefore, we have opted to use the type of Fe-oxide in the assemblage as a proxy for the oxidation state, since only 33.2% of the samples lack this information. The rationale for this categorisation is that hematite-bearing samples are probably more oxidised than magnetite–hematite-bearing ones, which, in turn are probably more oxidised than samples containing magnetite–ilmenite, ilmenite, or no Fe-oxide (Diener and Powell 2010). Complications arise when comparing rocks of different grade, or rocks that contain greater or lesser amounts of a silicate capable of incorporating significant Fe^{3+} (e.g., muscovite, biotite, etc.). Despite these caveats, this method provides a convenient first-order, observation-based proxy for

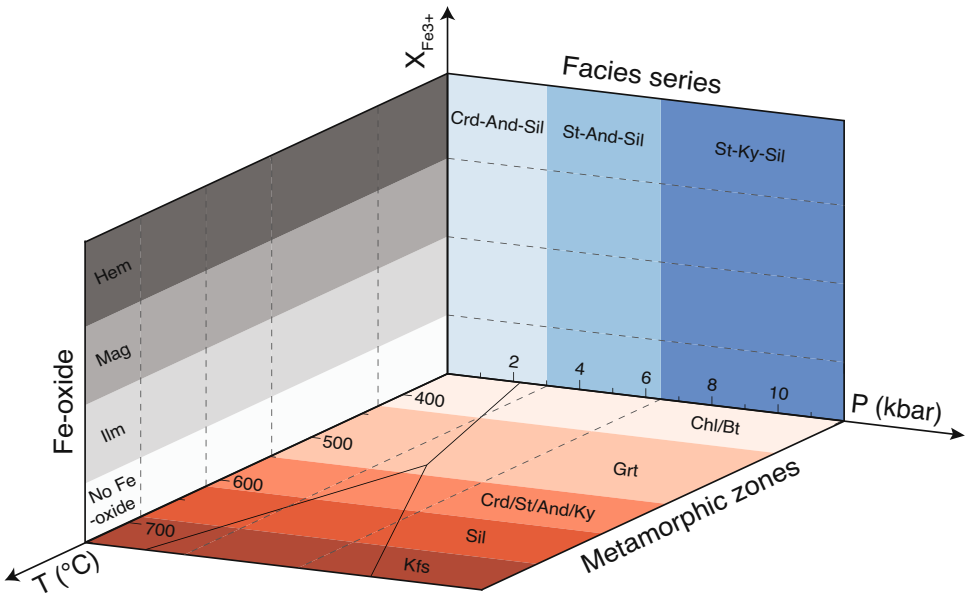

Fig. 2 Pressure (P, kbar), temperature (T, °C), and oxidation state (X_{Fe3+}) diagram illustrating the metamorphic zones, facies series, and Fe-oxide classifications used in this study. The aluminosilicate triple point calculated using the Holland and Powell (2011) dataset is shown for reference. Mineral abbreviations after Whitney and Evans (2010)

oxidation state. The reliability of this approach is assessed in more detail later in the paper.

Multiple Fe-oxides can coexist within the same rock. Our original attempt at classifying the samples based on the type of Fe-oxide led to eight categories (unknown, no Fe-oxide, Ilm, Ilm + Mag, Mag, Ilm + Mag + Hem, Mag + Hem, and Hem). Several of these had few (1–5) analyses and therefore some categories were combined in order to form five broader classifications: unknown; no Fe-oxide; Ilm-bearing; Mag-bearing (± Ilm); Hem-bearing (± Mag ± Ilm) (Fig. 2). Where authors simply stated the presence of opaque minerals (e.g., Atherton 1968; Kutsukake 1977; Miyashiro 1956, 1958; Stephenson 1979) or did not list any minor minerals as part of the assemblage (e.g., Snelling 1957), samples were included in the unknown category. Any sample where opaque minerals or Fe-oxides were not specifically identified, yet the authors noted other accessory minerals in the assemblage (e.g., Rt, Sph, Zr, Ap, Py, Po; Kwak 1968; Lundgren 1966), or the presence of Fe-oxides in different rocks in the same study (e.g., Mather 1970; Ono 1969), were included in the no Fe-oxide category. The type of Fe-oxide present in the sample is depicted on diagrams by the colour grey, with progressively darker shades indicating higher oxidation states (Fig. 2).

Figure 3a shows the percentage of minerals and rocks analysed for X_{Fe3+} in each of the five metamorphic zones. There are relatively few analyses in rocks from the Chl/Bt zone. Whole rock, white mica, and biotite analyses are well represented across a range of grade, whilst chlorite analyses are restricted to low metamorphic grade and staurolite analyses are restricted to intermediate metamorphic grade (Fig. 3a). Figure 3b shows the distribution of analyses as a function of the pressure-dependent facies series. The majority of analyses are from the Barrovian St–Ky–Sil series. Concerning the higher-P Buchan St-And-Sil facies series, a significant number of white mica, biotite, and chlorite analyses come from the West-central Maine sequence (Dyar et al. 1991, 2002; Guidotti et al. 1994; Guidotti and Dyar 1991; Moeller 1991). Figure 3c shows the distribution of analyses in relation to the type of Fe-oxide present in the rocks. In many samples, unfortunately, the Fe-oxide is unknown. The rarest samples are those that contain hematite.

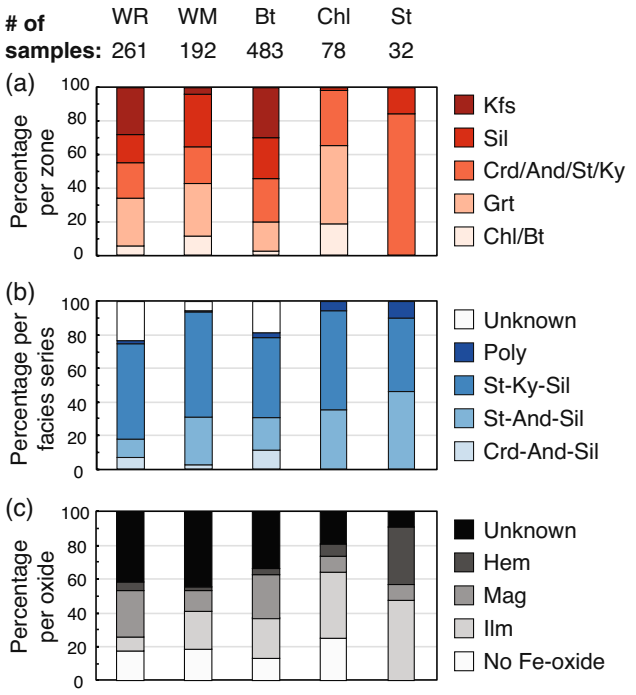

Fig. 3 Distribution of analyses as a percentage for each **a** metamorphic zone, **b** facies series, and **c** Fe-oxide type. The data are separated into five categories: X_{Fe3+} analyses of whole rock, white mica, biotite, chlorite, and staurolite. The total number of samples included in the database for each category is listed at the top

X_{Fe3+} and Fe^{3+} variation in metapelitic rocks and minerals

This study

In this section we analyse the database to elucidate broad patterns. Average ($\pm 1\sigma$) X_{Fe3+} values are listed in Table 2 and are as follows: whole rock, 0.23 ± 0.16 (261 analyses); biotite, 0.11 ± 0.08 (483); white mica, 0.55 ± 0.18 (192); chlorite, 0.08 ± 0.07 (78); and staurolite, 0.07 ± 0.06 (32). The average ($\pm 1\sigma$) number of Fe^{3+} cations per formula unit are also listed in Table 2 and are as follows: biotite, 0.28 ± 0.19 (460); white mica, 0.17 ± 0.13 (190); chlorite, 0.31 ± 0.27 (60); and staurolite, 0.20 ± 0.17 (25). The large standard deviations of some minerals highlight the wide range of X_{Fe3+} reported in the literature. To what degree this represents real variation in X_{Fe3+} of these minerals, rather than disparate results from a range of laboratories, is uncertain.

Variation in the Fe^{3+} contents and X_{Fe3+} of minerals and whole rock were considered in terms of the three main variables defined above. Figure 4 plots the mean, standard deviation, and range of X_{Fe3+} in rocks, biotite, and white mica classified by metamorphic grade, facies series, and type of Fe-oxide. Additionally, for biotite and white mica, Fig. 4b, c plots the mean, standard deviation, and range for the number of Fe^{3+} cations using the same classifications. The average X_{Fe3+} and Fe^{3+} contents for whole rock, biotite, and white mica as a function of the type of Fe-oxide are presented in Table 2. Chlorite and staurolite were not considered due to the small number of analyses and their relatively restricted stability ranges.

Mean whole rock X_{Fe3+} appears to decrease with increasing metamorphic grade (Fig. 4a; 0.31–0.18) as has been

Table 2 Mean ($\pm 1\sigma$) number of Fe^{3+} cations and X_{Fe3+} for whole rock and minerals

		All	No Fe-oxide	Ilmenite	Magnetite	Hematite
Whole rock	X_{Fe3+}	0.23 ± 0.15	0.21 ± 0.12	0.20 ± 0.09	0.22 ± 0.15	0.57 ± 0.21
White mica	X_{Fe3+}	0.55 ± 0.18	0.46 ± 0.19	0.49 ± 0.15	0.67 ± 0.16	0.62 ± 0.21
	Fe^{3+}	0.17 ± 0.13	0.17 ± 0.11	0.06 ± 0.03	0.19 ± 0.06	0.22 ± 0.07
Biotite	X_{Fe3+}	0.11 ± 0.08	0.08 ± 0.05	0.11 ± 0.06	0.13 ± 0.06	0.19 ± 0.09
	Fe^{3+}	0.28 ± 0.19	0.20 ± 0.14	0.30 ± 0.16	0.33 ± 0.16	0.33 ± 0.15
Chlorite	X_{Fe3+}	0.08 ± 0.07				
	Fe^{3+}	0.31 ± 0.27				
Staurolite	X_{Fe3+}	0.07 ± 0.06				
	Fe^{3+}	0.20 ± 0.17				

All = average of all analyses included in the database. No Fe-oxide, ilmenite, magnetite, and hematite = average for each the categories of Fe-oxide shown in Fig. 2

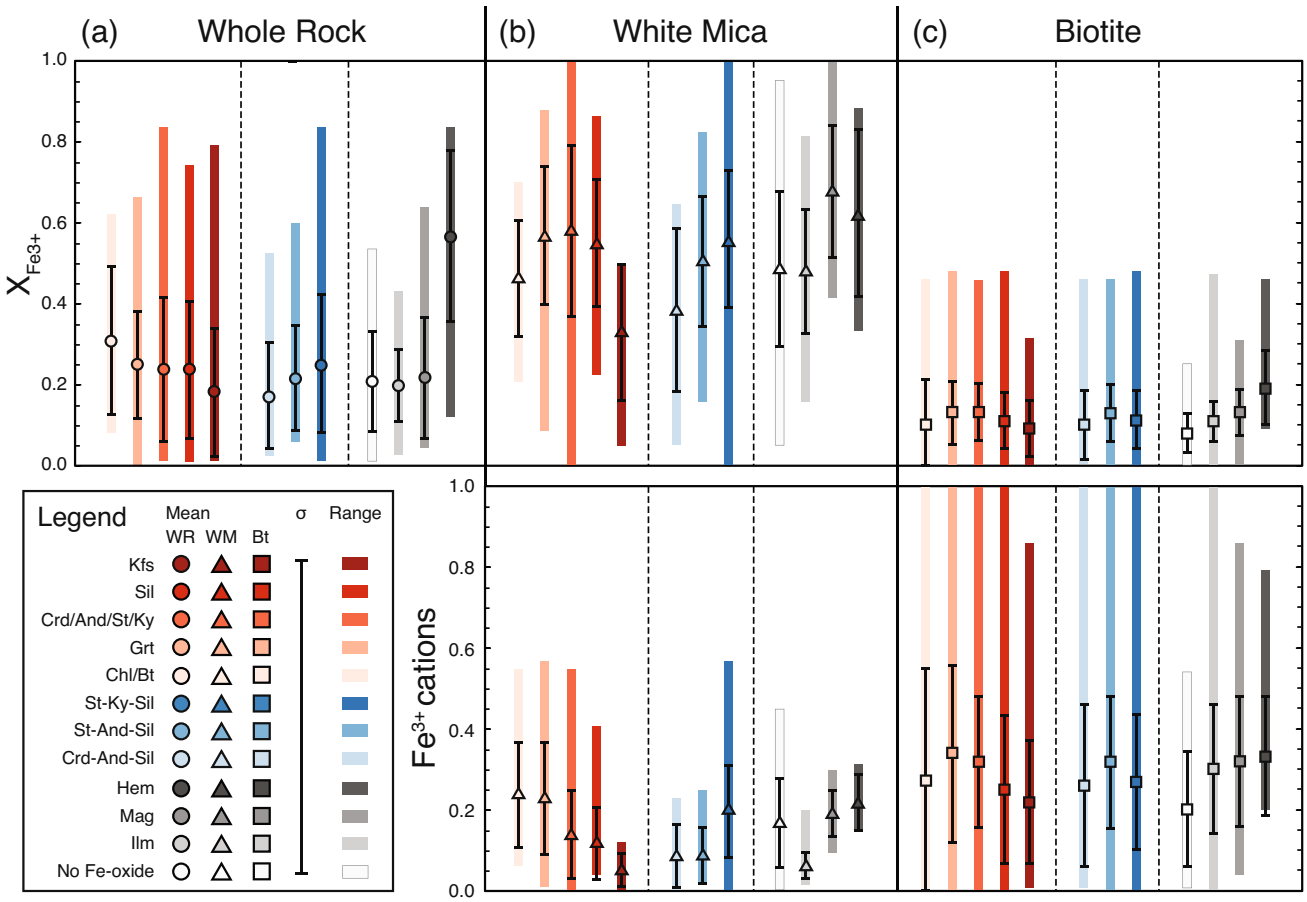

Fig. 4 X_{Fe3+} of **a** whole rock, **b** white mica, and **c** biotite, as well as the number of Fe^{3+} cations in **b** white mica, and **c** biotite, for different metamorphic zones, facies series, and types of Fe-oxide (colours as in Fig. 2). For each category the symbol represents the mean, the error bar one standard deviation, and the coloured rectangle the range

noted by several previous authors (Ague 1991; Barth 1936; Joyce 1970; Mason 1962; Schwarcz 1966; Shaw 1956). However, analysis of other compilations of whole rock data, specifically those from the Dalradian, has shown no correlation of X_{Fe3+} with grade (Atherton and Brotherton 1982; Leake 1958; Senior and Leake 1978; Yardley, 1977). Given that the averages presented here are well within uncertainty of each other and that there is a large spread in X_{Fe3+} for a given zone, it is not possible to say whether the apparent trend to lower values is significant. Whole rock X_{Fe3+} increases as a function of pressure (Fig. 4a). The slightly higher mean of the St–Ky–Sil series may be a result of a

higher proportion of hematite-bearing rocks being included in this category, as suggested by the wide range in Fig. 4a. The mean whole rock X_{Fe3+} value is similar for ilmenite- and magnetite-bearing rocks, as well as those with no Fe-oxide reported, but is considerably higher for hematite-bearing rocks (Fig. 4a; Table 2).

White mica X_{Fe3+} values are always higher than that of the whole rock and range from 0.0 to 1.0. Within overlapping ranges and standard deviations, mean white mica X_{Fe3+} is highest in the intermediate grade Crd/St/And/Ky zone, whereas the mean number of Fe^{3+} cations decreases with increasing metamorphic grade (Fig. 4b). Mean white mica X_{Fe3+} broadly increases as a function of pressure (Fig. 4b); the average number of Fe^{3+} cations for the lower pressure facies series is similar, but is about half the value of the St–Ky–Sil facies series white micas (Fig. 4b). White mica in magnetite- and hematite-bearing rocks has a higher mean X_{Fe3+} than in ilmenite and Fe-oxide-free rocks (Fig. 4b; Table 2). The mean number of Fe^{3+} cations in white mica similarly increases from ilmenite- to magnetite- to hematite-bearing rocks (Fig. 4b; Table 2). Average X_{Fe3+} and Fe^{3+} cations in biotite show no consistent trends with respect to metamorphic grade and facies series. However, both show a slight correlation as a function of Fe-oxide, with maximum values in hematite-bearing rocks (Fig. 4c; Table 2).

Comparison to other studies

Previous studies have demonstrated that metapelites of the same metamorphic grade containing hematite have higher whole rock X_{Fe3+} contents than ilmenite–magnetite-bearing rocks (Chinner 1960; Hounslow and Moore 1967), as found here. No previous studies that we are aware of have compared whole rock X_{Fe3+} contents amongst magnetite-bearing, ilmenite-bearing, and Fe-oxide-free rocks.

The only previous systematic study of Fe^{3+} in metapelitic minerals is that of Guidotti, Dyar, and others from across a Grt–St–Sil–Kfs sequence in West-central Maine (Dyar 1990; Dyar et al. 1991, 2002; Guidotti et al. 1994; Guidotti and Dyar 1991). In this region, the average ($\pm 1\sigma$) X_{Fe3+} of biotite was 0.11 ± 0.05 for 45 ilmenite-bearing rocks, 0.24 ± 0.05 for five magnetite-bearing rocks, and 0.46 in a single hematite-bearing rock. Comparatively, the average ($\pm 1\sigma$) X_{Fe3+} of white mica was 0.45 ± 0.11 for twelve graphite–ilmenite-bearing schists, 0.72 ± 0.07 for five ilmenite–magnetite-bearing samples, and 0.82 in a single hematite-bearing rock. In our database, the average X_{Fe3+} values of biotite for magnetite- and hematite-bearing samples are significantly lower than those reported by Dyar (1990). For white mica, our values are similar to those of Guidotti et al. (1994), apart from our average X_{Fe3+} for hematite-bearing samples which is 0.20 lower than their single sample.

Biotite is the only mineral considered here for which researchers have previously estimated Fe^{3+} contents from recalculated EPMA data based on stoichiometric constraints. Dymek (1983) developed an iterative cation-based normalisation procedure that eliminates excess charge associated with Ti^{4+} and Al^{3+} using octahedral vacancies, and then estimates Fe^{3+} based on the difference between the total positive charge and 22 oxygens. However, this calculation assumes that titanium is incorporated at the octahedral site through vacancies and not via deprotonation, in contrast to the studies noted earlier, making these Fe^{3+} estimates equivocal (Cesare et al. 2003; Dyar et al. 1993a; Waters and Charnley 2002). Li et al. (2020) used an Fe^{3+} estimation method based on principal components regression; we tested its ability to reproduce the X_{Fe3+} contents of the biotite analyses in our database. To do so, our separate determinations of Fe_2O_3 and FeO were combined into FeO^{total} and the amount of Fe^{3+} in biotite calculated using the spreadsheet provided by Li et al. (2020). Figure 5 plots the observed X_{Fe3+} in biotite against that calculated using the Li et al. (2020) method; samples for which X_{Fe3+} was exactly predicted by the spreadsheet lie on the 1:1 line. We find a poor fit between the observed and predicted X_{Fe3+}.

Phase equilibrium modelling considerations

The next part of this study compares our observations from the natural database with the predictions of thermodynamic modelling. The following section outlines the average bulk composition used for phase diagram calculations,

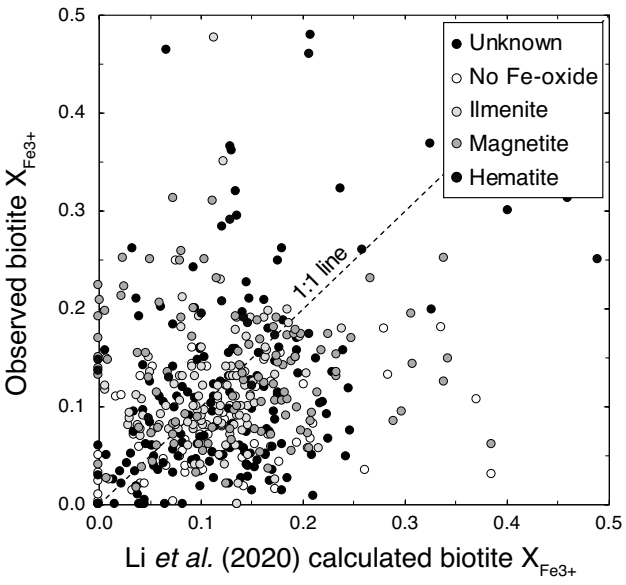

Fig. 5 Observed X_{Fe3+} in biotite vs. the predicted X_{Fe3+} in biotite calculated using the method of Li et al. (2020)

overviews the various substitution mechanisms by which Fe^{3+} is incorporated in minerals, and summarises the different thermodynamic solution models and datasets available for Fe^{3+}-bearing phases. Finally, we discuss the various types of phase equilibrium modelling calculation conducted, before contrasting thermodynamic predictions to the natural data in a subsequent section.

Average bulk composition

Phase diagram calculations were performed for the average composition of the 261 whole rock compositions in the database. This bulk composition is provided in Table 3 alongside the mean whole rock compositions determined by Shaw (1956), Ague (1991), and Atherton and Brotherton (1982). H_2O and CO_2 have been removed and values renormalised to 100% to provide a uniform basis for comparison. The weight per cent oxide concentrations for major elements in our bulk composition are close to those of previous authors for average pelitic rocks. This average composition was converted to mole per cent and an apatite correction was applied to remove P_2O_5 and a corresponding stoichiometric amount of CaO. The value of $X_{Fe3+} = 0.23$ in our average metapelite is lower than in Shaw's (1956) low-grade pelite ($X_{Fe3+} = 0.46$) and Ague's (1991) slate/shale ($X_{Fe3+} = 0.40$), but similar to Shaw's (1956) high-grade pelite ($X_{Fe3+} = 0.28$) and Ague's (1991) amphibolite–facies pelite ($X_{Fe3+} = 0.25$). It also lies between the values for average Dalradian Buchan pelite ($X_{Fe3+} = 0.17$) and average Dalradian Barrovian pelite ($X_{Fe3+} = 0.32$) presented by Atherton and Brotherton (1982).

Fe^{3+} substitution mechanisms

Here we briefly review the crystallographic sites and exchange mechanisms by which Fe^{3+} is incorporated in white mica, biotite, chlorite, and staurolite. For white mica, biotite, and chlorite, most studies (including the present one) assume that Fe^{3+} replaces Al^{3+} in an octahedral site. However, some authors debate which site or sites Fe^{3+} can occur in, as well as the various ways in which the excess charge associated with this substitution is accommodated (see "Mineral formulae recalculation" section). In biotite, Guidotti and Dyar (1991) suggested that $8 \pm 3\%$ of total Fe is tetrahedral Fe^{3+}, whilst 4–13% of total Fe is octahedral Fe^{3+}. However, these site-assignments were subsequently questioned (Dyar 1993; Rancourt 1993; Rancourt et al. 1992), and when these data were refit, Fe^{3+} was assigned exclusively to the octahedral site (Dyar et al. 2002). As previously discussed, some authors have suggested that the extra charge associated with Fe^{3+} in an octahedral site is accommodated by deprotonation, but it is now thought that deprotonation related to Fe^{3+} is minor compared to Ti^{4+}

Table 3 The average database bulk rock composition determined in this study compared to the averages of Shaw (1956, table 9), Ague (1991, table 2), and Atherton and Brotherton (1982, table 4)

Name (source)	#	SiO_2	TiO_2	Al_2O_3	Fe_2O_3	FeO	MnO	MgO	CaO	Na_2O	K_2O	P_2O_5	X_{Mg}	X_{Fe3+}
Metapelite database average (this study)	252 (261)	60.77	0.97	18.43	1.91	5.11	0.12	2.58	1.29	1.79	3.80	0.15	0.45	0.23
Low grade pelitic average (Shaw 1956)	85 (85)	63.97	0.91	17.74	3.23	3.39		2.81	2.33	1.85	3.78		0.60	0.46
High grade pelitic average (Shaw 1956)	70 (70)	65.33	0.81	17.85	2.06	4.84		2.38	1.28	2.02	3.45		0.46	0.28
Shale/slate average (Ague 1991)	105 (105)	63.77	0.80	18.02	3.10	4.21	0.10	2.84	1.53	1.64	3.85	0.15	0.55	0.40
Amphibolite average (Ague 1991)	161 (161)	57.97	1.08	20.80	2.38	6.48	0.19	3.33	1.59	1.85	4.14	0.20	0.48	0.25
Barrovian average (Atherton and Brotherton 1982)	192 (177)	62.21	1.05	19.72	2.80	5.00	0.12	2.33	0.95	2.13	3.68		0.46	0.32
Buchan average (Atherton and Brotherton 1982)	38 (37)	60.15	1.12	20.08	1.48	6.85	0.12	2.93	1.61	2.38	3.27		0.44	0.17

H_2O and CO_2 omitted. Values in weight per cent oxide, renormalised to 100%. #= Total number of analyses included in the averaged SiO_2, Al_2O_3, MgO, CaO, Na_2O, and K_2O values. The number in parentheses is the number of analyses included in the averaged FeO and Fe_2O_3 values and thus whole rock X_{Fe3+}. $X_{Mg} = Mg/(Mg + Fe^{2+})$ and $X_{Fe3+} = Fe^{3+}/(Fe^{3+} + Fe^{2+})$ in moles

(Cesare et al. 2003; Waters and Charnley 2002). In muscovite, $Fe^{3+} = Al^{VI}$ is the dominant substitution by which Fe^{3+} is incorporated, with only a minor contribution from deprotonation (Dyar et al. 1993a; Guidotti and Sassi 1998a, b). For chlorite, whilst Fe^{3+} typically replaces Al^{VI}, it may also substitute for octahedral Fe^{2+} or Mg^{2+} as part of a deprotonation substitution (Lempart et al. 2018, 2020; Masci et al. 2019; Walshe 1986). In staurolite, Fe^{3+} replaces Al^{3+} in the tetrahedral site (Dyar et al. 1991).

Fe^{3+} in thermodynamic databases

Of the four minerals considered here, attention has been focussed on thermodynamic properties of Fe^{3+} end members in biotite and chlorite. In biotite, Vieillard (1994) predicted the enthalpy of formation for ferri–annite and ferri–phlogopite in which Fe^{3+} replaces Al^{3+} on the tetrahedral site. In contrast, White et al. (2000, 2005, 2007) and Tajčmanová et al. (2009) considered that Fe^{3+} resides exclusively on the octahedral M1 site and consequently use a single Fe^{3+} end member [fbi = $KMg_2Fe^{3+}Al_2Si_2O_{10}(OH)_2$]. These studies derived the equation of state for fbi using stoichiometrically weighted linear combinations of the properties of phases with known thermodynamic properties, specifically eastonite, corundum, and hematite from the Holland and Powell (1998) dataset (fbi = Eas – ½ Crn + ½ Hem). White et al. (2014a) used the same Fe^{3+} end member but derived the equation of state with thermodynamic properties for eastonite, grossular, and andradite from the Holland and Powell (2011) dataset (fbi = Eas – ½ Grs + ½ Adr).

For chlorite, Walshe (1986) included two Fe^{3+} end members in his solid solution model. In the first of these Fe^{3+} replaces Al^{3+} on the tetrahedral and octahedral sites ($Fe^{2+}{}_5Fe^{3+}{}_2Si_3O_{10}(OH)_8$), whilst in the second, Fe^{3+} is incorporated on the octahedral site via deprotonation ($Fe^{2+}{}_4Fe^{3+}Al_2Si_3O_{11}(OH)_7$). White et al. (2014a) used a single Fe^{3+} end member in chlorite (f3clin = $Mg_5Fe^{3+}AlSi_3O_{10}(OH)_8$), deriving the equation of state for f3clin using the thermodynamic properties from Holland and Powell (2011) for clinochlore, grossular, and andradite (f3clin = Clc – ½ Grs + ½ Adr). Based on examination of Fe^{3+} and OH contents in chlorite from a large natural dataset, Masci et al. (2019) suggested that for thermodynamic modelling at least two ferric end-members are necessary: one with low Fe content where Fe^{3+} replaces Al and one where Fe^{3+} is incorporated by deprotonation. In contrast, some authors have chosen not to derive equations of state for Fe^{3+} end members in chlorite, since variation in X_{Fe3+} is argued to be systematic and continuous with temperature, meaning that the incorporation of Fe^{3+} is intrinsically included in the derivation of other standard state and solution properties (Lanari et al. 2014; Vidal et al. 2005, 2006).

To our knowledge, White et al. (2014a) are the only authors to propose thermodynamic properties for Fe^{3+} end members in muscovite and staurolite. They considered Fe^{3+} to be partitioned onto the octahedral site in muscovite, and the tetrahedral site in staurolite, using a single Fe^{3+} end member for each mineral (fmu, $KFe^{3+}Al_2Si_3O_{10}(OH)_2$; msto, $Fe^{3+}{}_2Mg_4Al_{16}Si_{7.5}O_{44}(OH)_4$). White et al. (2014a) derived the equations of state for fmu and msto using the thermodynamic properties from Holland and Powell (2011) for muscovite, staurolite, grossular, and andradite (fmu = Ms – ½ Grs + ½ Adr; msto = St – ½ Grs + ½ Adr).

Choice of thermodynamic database

The thermodynamic datasets of Berman (1988) and Holland and Powell (1998, 1990) have relatively few Fe^{3+}-bearing end members for silicate phases, as well as few associated solution models describing mixing between end members. Whilst some other solution models exist for chlorite and biotite (e.g., Vieillard 1994; Walshe 1986), the properties of end members are derived from thermodynamic data that are inconsistent with one another and thus cannot be combined. Of the thermodynamic databases currently available, only the dataset of Holland and Powell (2011) and associated solution models of White et al. (2014a) incorporate enough Fe^{3+} end members to simulate natural Fe^{3+}-bearing phase equilibria. We therefore conducted phase equilibrium modelling in the internally consistent dataset of Holland and Powell (2011; update dataset 6.2, 6th February 2012) with the following solution models: chlorite, biotite, garnet, chloritoid, staurolite, cordierite, orthopyroxene, muscovite, paragonite, margarite, and silicate melt (White et al. 2014a, b); plagioclase and K-feldspar (Holland and Powell 2003; ternary feldspar, Cbar1 field); epidote (Holland and Powell 2011); ilmenite–hematite (White et al. 2000, 2014a, b); magnetite–spinel (White et al. 2002). Pure phases included quartz, albite, rutile, sphene, and the aluminosilicates. H_2O was assumed to be in excess.

Calculation details

Phase diagrams were computed in the 11-component MnNCKFMASHTO system ($MnO–Na_2O–CaO–K_2O–FeO–MgO–Al_2O3–SiO_2–H_2O–TiO_2–O_2$), using Theriak–Domino (De Capitani and Brown 1987; De Capitani and Petrakakis 2010; version 11th February 2015, modified by D. Tinkham). First, our average bulk composition ($X_{Fe3+} = 0.23$) was used to calculate a P–T equilibrium assemblage diagram (Fig. 6a). Second, an isobaric T-X_{Fe3+} (whole rock) equilibrium assemblage diagram at a pressure of 5 kbar was constructed (Fig. 6b). In this diagram, the proportions of Fe^{2+} and Fe^{3+} were varied between $X_{Fe3+} = 0.0$ and $X_{Fe3+} = 1.0$, with all

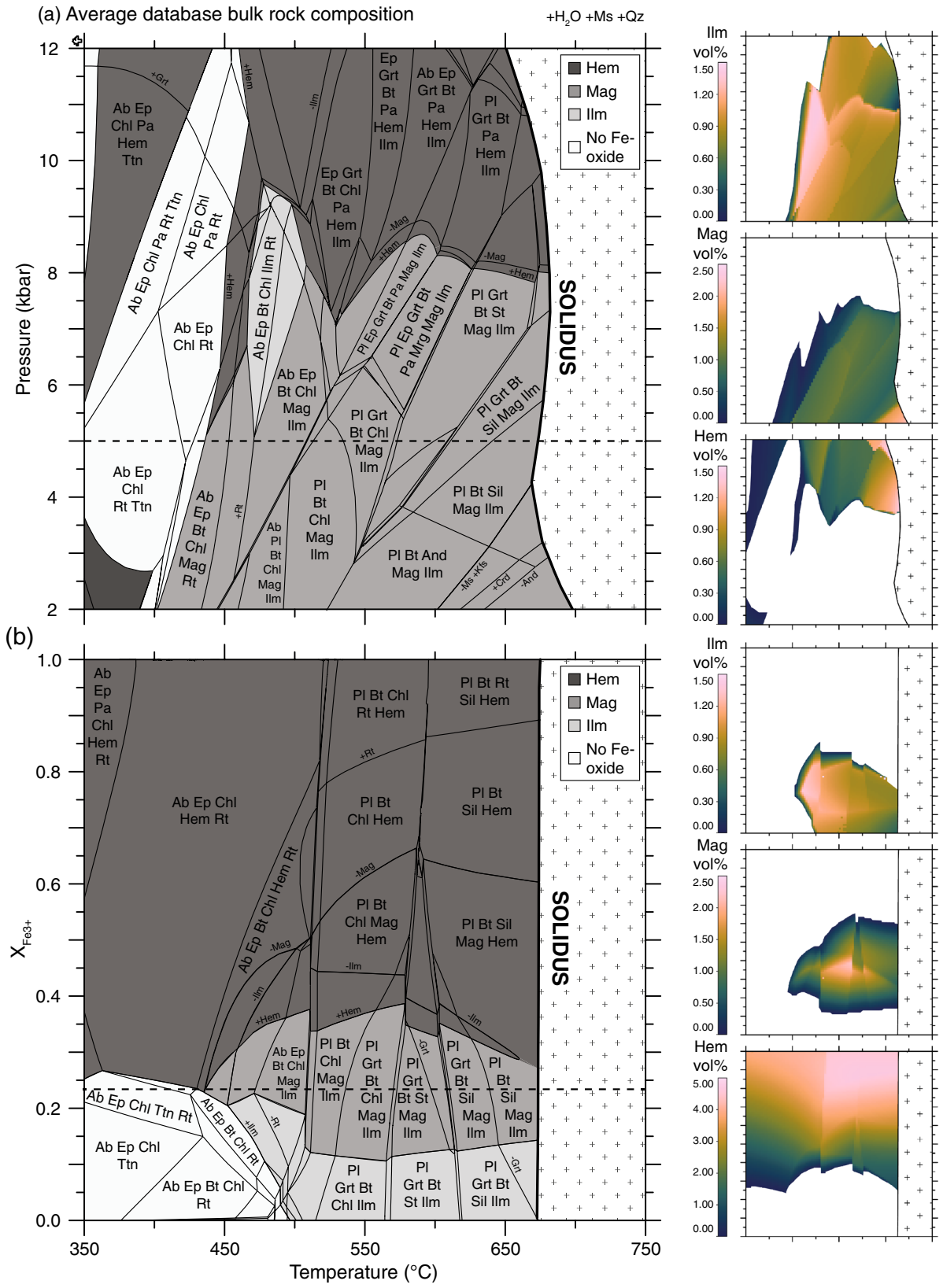

Fig. 6 **a** P–T and **b** T-X_{Fe3+} phase diagrams calculated using the average bulk composition listed in Table 3. The cross patterned field denotes the domain of predicted melt-bearing assemblages. The dashed lines show the pressure and X_{Fe3+} content at which the corresponding diagram was calculated. Smaller diagrams depict the change in volume per cent of ilmenite, magnetite, and hematite

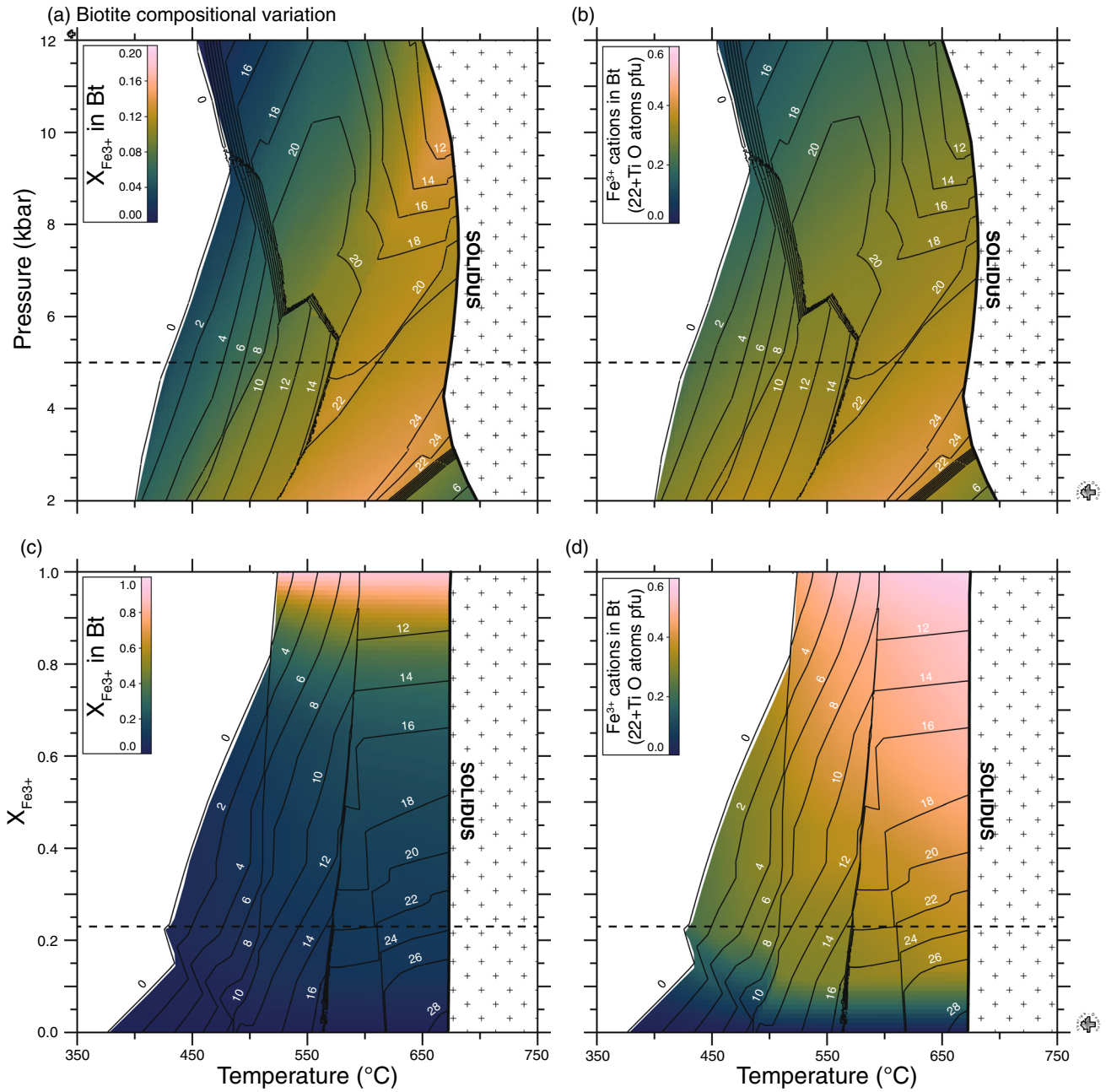

Fig. 7 Change in biotite **a**, **c** X_{Fe3+} and **b**, **d** Fe^{3+} cations with **a**, **b** P–T and **c**, **d** T-X_{Fe3+} conditions. Isomodes are plotted as black lines with associated white numbers showing the volume per cent of the mineral present

other elements kept at the same values. The pixelmaps routine of Domino was utilised to calculate the modal abundances and compositions of minerals across these two diagrams. The predicted number of Fe^{2+} and Fe^{3+} cations pfu and in turn the X_{Fe3+} of each mineral, were then determined. The scientific colour map 'batlow' (Crameri 2021) is used for pixelmaps in this study (Crameri et al. 2020).

To gain further insight into the interplay of pressure, temperature, and oxidation state, P–T diagrams like that shown in Fig. 6a were constructed for ten separate whole rock X_{Fe3+} values between 0.0 and 0.9 with an interval of 0.1. Calculations for a whole rock X_{Fe3+} of 1.0 were not included, because the highest whole rock X_{Fe3+} value in our database is 0.84. Each P–T diagram was gridded with 11 × 11 pixels spaced 40 °C and 1 kbar apart, resulting in 121 datapoints per map and 1210 datapoints total. At every point, the model predicts the stable mineral assemblage, including Fe-oxides, and the mineral compositions for which each Fe^{3+}-bearing mineral will have an associated X_{Fe3+}. Using the predicted Fe-oxide, we categorised each point according to the scheme

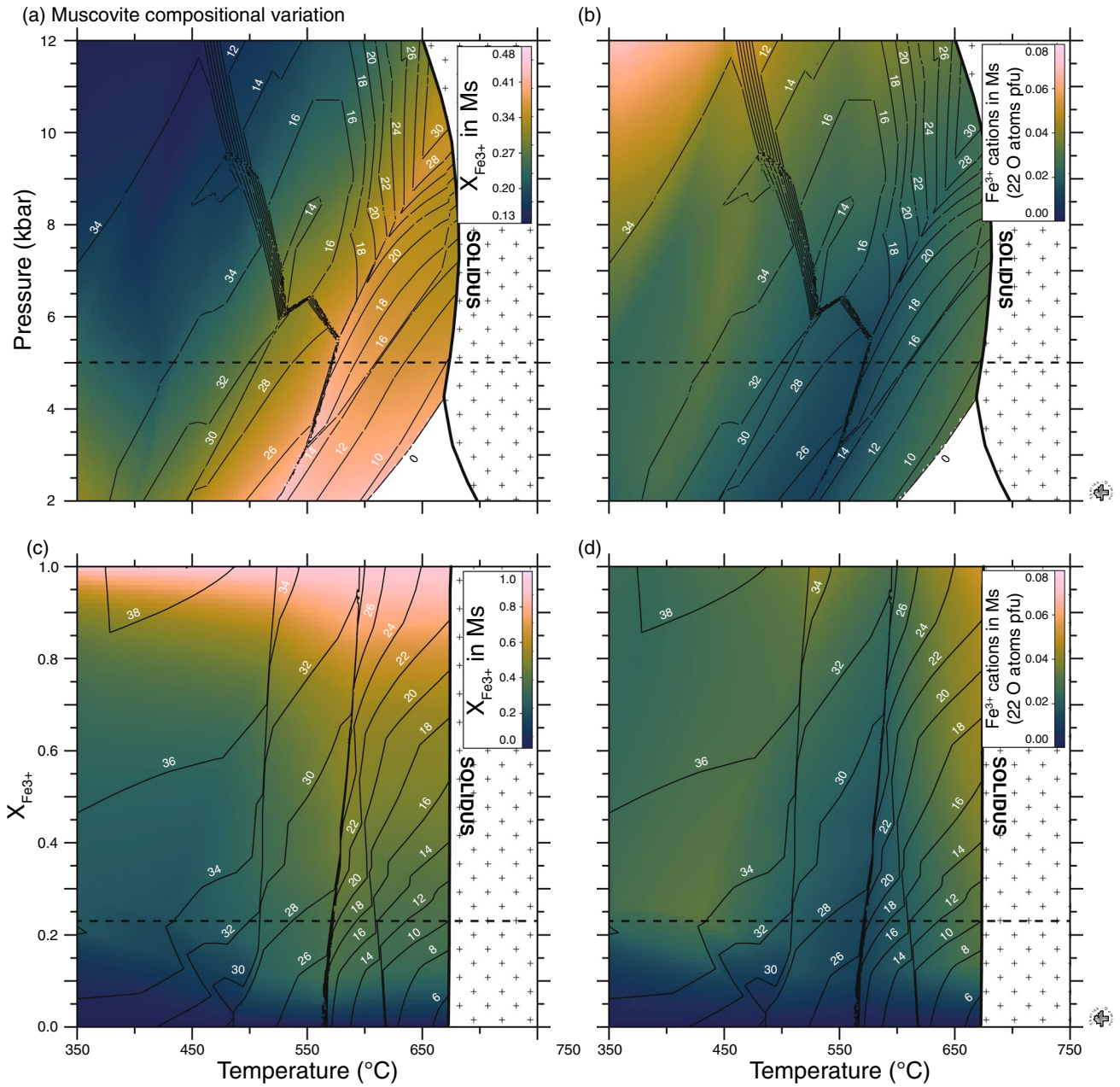

Fig. 8 As for Fig. 7, but for muscovite

presented in the "Data classification with respect to pressure, temperature, and oxidation state" section. We then grouped all the points into one of the Fe-oxide categories described above for the natural data (e.g., magnetite), and calculated the predicted mean, standard deviation, and range in X_{Fe3+} and the number of Fe^{3+} cations for the whole rock and mineral compositions (Ms, Bt, Chl, and St).

Phase equilibrium modelling results and comparison to natural data

Predicted Fe-oxide

Figure 6 shows the P–T and T-X_{Fe3+} equilibrium assemblage diagrams produced for our average metapelite composition, with the shades of grey highlighting which Fe-oxide is present, according to the scheme presented in the "Data classification with respect to pressure, temperature, and oxidation

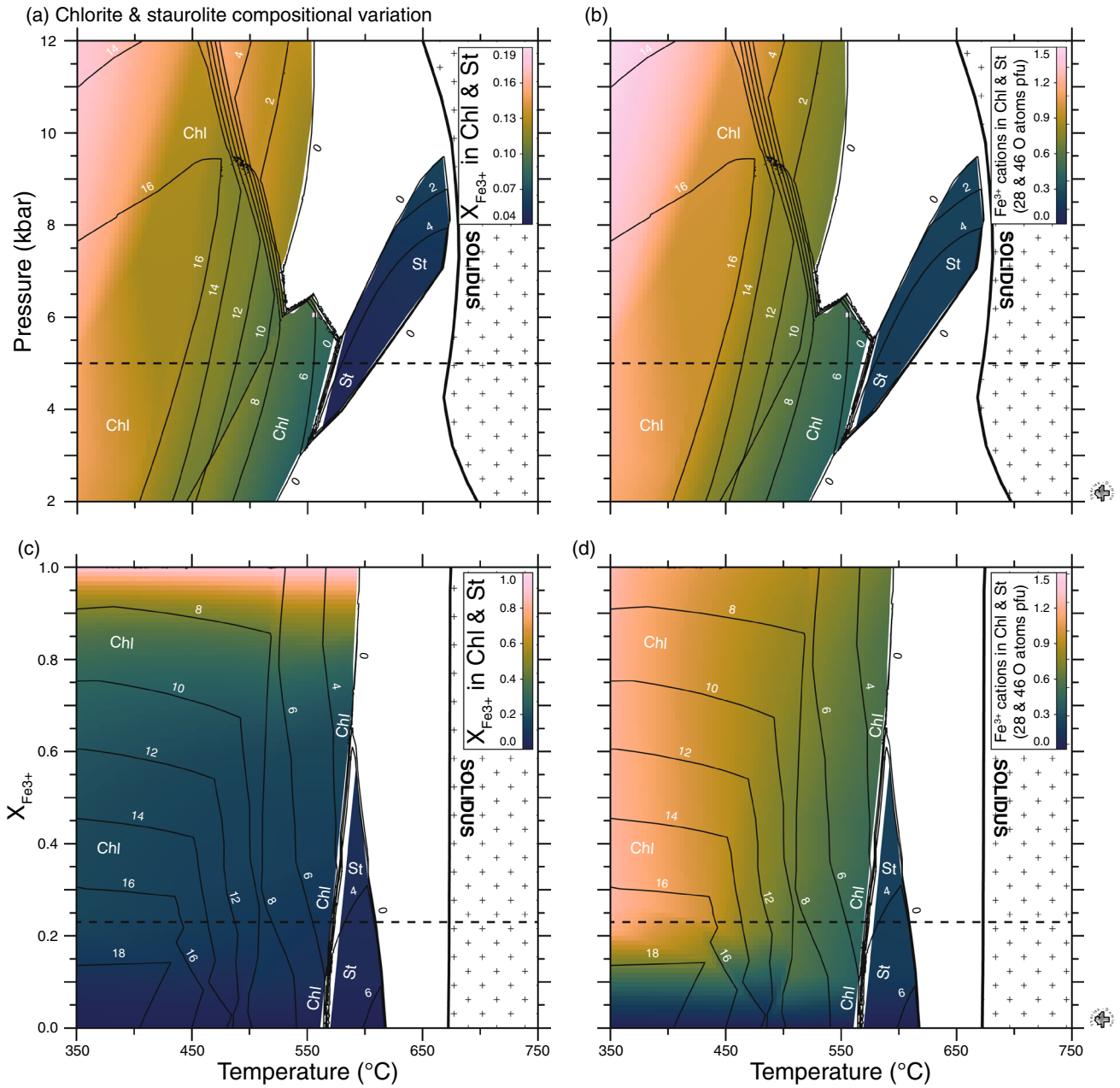

Fig. 9 As for Fig. 7, but for chlorite and staurolite

state" section. The dashed line on Fig. 6a shows the 5 kbar pressure used to calculate the isobaric phase diagram in Fig. 6b, whilst the dashed line on Fig. 6b shows the average rock X_{Fe3+} value. Magnetite-bearing assemblages are stable at pressures below ~ 8 kbar and 450–650 °C, whilst hematite-bearing assemblages are stable above ~ 8 kbar (Fig. 6a). At temperatures below ~ 450 °C either no Fe-oxide is predicted to be present, or a small amount of hematite is predicted (< 0.3%; Fig. 6a). A small field where only ilmenite is predicted to be stable lies between 5 and 9 kbar and 450–500 °C. The predicted volume proportion of Fe-oxides is < 2% for the entire range of P–T conditions (Fig. 6a).

Referring to Fig. 6b, no Fe-oxide phase is predicted at low temperatures and oxidation states because epidote, a mineral with considerable Fe^{3+}, is present (Fig. 6b). Ilmenite is the only oxide at 450–650 °C and X_{Fe3+} < 0.1, forming 0.6–1.2 volume per cent of the predicted assemblage. Magnetite enters the assemblage above X_{Fe3+} = 0.1 and reaches a maximum volume of ~ 2% at X_{Fe3+} = 0.5 and 550 °C. Hematite is predicted to be stable at X_{Fe3+} > 0.3 and occurs with both ilmenite and magnetite at X_{Fe3+} = 0.4 (Fig. 6b).

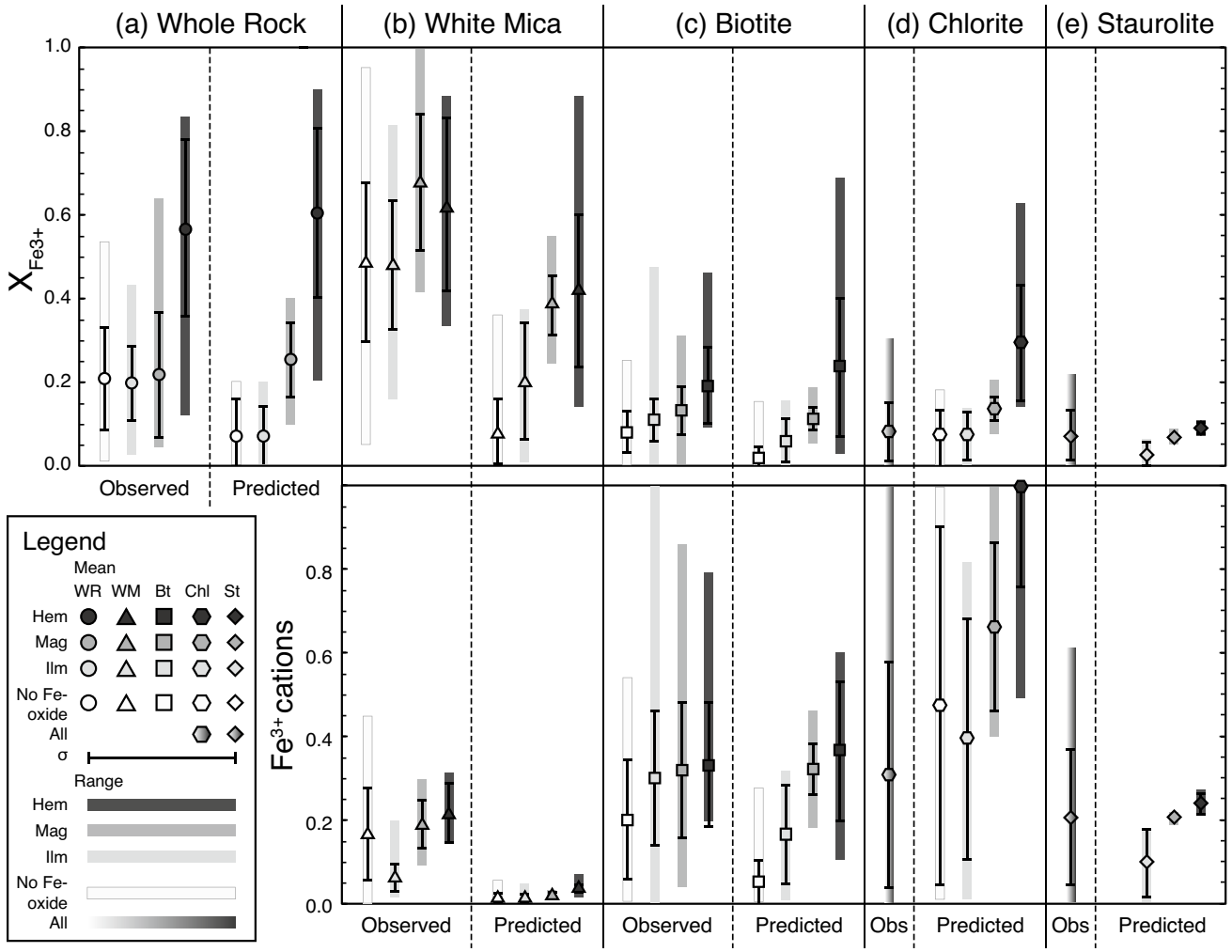

Fig. 10 Comparison of the observed and predicted X_{Fe3+} and number of Fe^{3+} cations in **a** whole rock, **b** white mica/muscovite, **c** biotite, **d** chlorite, and **e** staurolite for different types of Fe-oxide. Observed chlorite and staurolite X_{Fe3+} values are not separated by the type of Fe-oxide due to the small number of analyses. For each category the symbol represents the mean, the error bar one standard deviation, and the coloured rectangle the range, as in Fig. 4

Hematite is the only Fe-oxide predicted to be stable at $X_{Fe3+} > 0.6$ and its volume percent increases from ~ 2% at $X_{Fe3+} = 0.4$ to ~ 5% at $X_{Fe3+} = 1.0$ (Fig. 6b). The stability of some silicate phases also changes as a result of the whole rock X_{Fe3+}, however, this is probably a result of increasing X_{Mg} associated with a reduction in Fe^{2+} as X_{Fe3+} increases (c.f., Diener and Powell 2010). The temperature interval over which staurolite and garnet are stable decreases with increasing whole rock X_{Fe3+} until neither is present above $X_{Fe3+} = 0.6$ (Fig. 6b).

Figure 6b can be compared with the T-X_{Fe3+} diagram in figure 4 of Diener and Powell (2010). Their diagram was constructed for a typical pelitic composition, using the older dataset of Holland and Powell (1998; update ds55, 4th August 2004), and the following solution models: garnet, biotite, and silicate melt (White et al. 2007); plagioclase and K-feldspar (Holland and Powell 2003; ternary feldspar, Cbar1 field); orthopyroxene and magnetite–spinel (White et al. 2002); muscovite–paragonite (Coggon and Holland 2002); ilmenite–hematite (White et al. 2000); chloritoid, staurolite, cordierite, and epidote (Holland and Powell 1998). Fewer of these silicate solution models incorporate Fe^{3+} end members (only garnet, biotite, orthopyroxene, and epidote) and the average predicted X_{Fe3+} in biotite is significantly lower than that predicted using the solution models of White et al. (2014a) in combination with the dataset of Holland and Powell (2011). The result is that the predicted stability fields and modal abundances of the Fe-oxides differ from Fig. 6b of this study because more Fe^{3+} must be included in the Fe-oxide phases. For example, at 550 °C, magnetite and hematite are predicted to be stable at significantly lower whole rock X_{Fe3+} contents in their diagram

compared to ours (0.05 vs. 0.10 for magnetite and 0.25 vs. 0.35 for hematite).

Predicted mineral X_{Fe3+} and Fe^{3+}

Figures 7, 8, and 9 display the predicted number of Fe^{3+} cations and X_{Fe3+} values, across the P–T and T-X_{Fe3+} equilibrium assemblage diagrams in Fig. 6, for biotite, muscovite, and chlorite/staurolite, respectively. These are contoured with modal abundance isopleths for each mineral in order to elucidate if any changes are associated with the volume percent of the phase predicted.

In biotite, gradual increases with temperature of X_{Fe3+} from ~ 0.03 to ~ 0.17 and in Fe^{3+} cations from ~ 0.10 to ~ 0.40, are punctuated by more abrupt changes at the Ep-out and Chl-out lines (Fig. 7a, b). At lower pressures (< 6 kbar), increases in the X_{Fe3+} and the number of Fe^{3+} cations in biotite correlate with increases in its modal abundance; however, at higher pressures (> 6 kbar) X_{Fe3+} and the number of Fe^{3+} cations in biotite are more uniform despite changes in modal abundance (Fig. 7a, b). There is no significant variation in the X_{Fe3+} and number of Fe^{3+} cations in biotite as a function of pressure. Predicted biotite Fe^{3+} cations and X_{Fe3+} increase with increasing whole rock X_{Fe3+}, whereas the modal abundance of biotite decreases (Fig. 7c, d). The predicted rates of increase in biotite Fe^{3+} cations and X_{Fe3+} with respect to whole rock X_{Fe3+} are different. The number of Fe^{3+} cations in biotite rapidly increases at lower whole rock X_{Fe3+} (Fig. 7d), whilst X_{Fe3+} in biotite increases most rapidly at higher whole rock X_{Fe3+} (Fig. 7c).

In muscovite, X_{Fe3+} is predicted to increase from ~ 0.20 to ~ 0.50 with increasing temperature and decreasing pressure (Fig. 8a), whilst the number of Fe^{3+} cations contemporaneously decreases from ~ 0.06 to ~ 0.01 (Fig. 8b). Muscovite has the greatest X_{Fe3+} and lowest number of Fe^{3+} cations at the Chl-out reaction, and the lowest X_{Fe3+} and greatest number of Fe^{3+} cations at > 10 kbar and < 450 °C (Fig. 8a, b). No correlation is found across P–T space between muscovite's modal abundance and its number of Fe^{3+} cations or X_{Fe3+}. However, both the predicted X_{Fe3+} of muscovite and its modal abundance increase with increasing whole rock X_{Fe3+} (Fig. 8c). Above whole rock X_{Fe3+} = 0.2, the number of Fe^{3+} cations predicted in muscovite shows greater variation with temperature than with whole rock X_{Fe3+} (Fig. 8d).

In chlorite, X_{Fe3+} decreases from ~ 0.19 to ~ 0.07 with increasing temperature, whilst the number of Fe^{3+} cations decreases from ~ 1.5 to ~ 0.5 (Fig. 9a, b). At lower pressures (< 6 kbar), increases in the number of Fe^{3+} cations and X_{Fe3+} in chlorite correlate with increasing modal abundance; however, at higher pressures (> 6 kbar) values are more uniform despite change in chlorite's modal abundance (Fig. 9a, b). There is negligible change in the number of Fe^{3+} cations and X_{Fe3+} in chlorite with pressure. Predicted chlorite Fe^{3+} cations and X_{Fe3+} increase with increasing whole rock X_{Fe3+}, whilst its modal abundance decreases (Fig. 9c, d). The predicted rates of increase in the number of Fe^{3+} cations and X_{Fe3+} are comparable to those previously described for biotite.

The number of Fe^{3+} cations in staurolite and its X_{Fe3+} remain constant (~ 0.2 and ~ 0.05; Fig. 9a, b). No correlation is found between the modal abundance of staurolite and either its number of Fe^{3+} cations or X_{Fe3+} across P–T space. The number of Fe^{3+} cations and X_{Fe3+} in staurolite remain relatively unchanged with whole rock X_{Fe3+}, however, its modal abundance decreases with increasing whole rock X_{Fe3+} (Fig. 9c, d).

Comparison of models to nature

Figure 10a compares means of the modelled whole rock X_{Fe3+} values that correspond to the Fe-oxide predicted (e.g., ilmenite or magnetite), with those observed in our database (Fig. 4). Mean whole rock X_{Fe3+} values where no Fe-oxide or only ilmenite were predicted (~ 0.08), are lower than the mean whole rock X_{Fe3+} determined from our database (~ 0.2). In contrast, the mean whole rock X_{Fe3+} values where magnetite or hematite were predicted are close to the mean whole rock X_{Fe3+} found in our database. It should be noted that a limitation of this assessment is that a single average bulk composition was used in the predictions, with only whole rock X_{Fe3+} varied, whereas the natural data integrate results from a wider range of rock compositions.

Figure 10b, c, d, e compares the predicted number of Fe^{3+} cations and X_{Fe3+} values in white mica, biotite, chlorite, and staurolite with those observed in our database (Fig. 4; Table 2). Mean muscovite X_{Fe3+} values where no Fe-oxide, or only ilmenite, were predicted, are lower than those where magnetite or hematite were predicted, as observed in our natural database (Figs. 8c, d, 10b). However, the mean predicted values of X_{Fe3+} and the number of Fe^{3+} cations in muscovite are always lower than those observed (Fig. 10b). For biotite, the models predict the observed increase in the number of Fe^{3+} cations and X_{Fe3+} with increasing whole rock X_{Fe3+} and with Fe-oxide present (Figs. 7c, d, 10c). Whilst the mean predicted values of X_{Fe3+} in biotite for different types of Fe-oxide broadly match those observed, the mean number of predicted Fe^{3+} cations is only similar when magnetite and hematite are the predicted Fe-oxide (Fig. 10c). The predicted variations in biotite Fe^{3+} cations and X_{Fe3+} contents as a function of pressure and temperature are not observed in the natural database (Figs. 4, 7). Predicted mean X_{Fe3+} values of staurolite and chlorite are generally low (< 0.2), in good agreement with the few analyses included in the database (Fig. 10d, e); however, both the mean number of predicted Fe^{3+} cations and the range of X_{Fe3+} in chlorite extend to higher values than those observed

(Fig. 10d). The predicted decrease in chlorite X_{Fe3+} with increasing temperature shown in Fig. 9 cannot be corroborated by the small number of data in our database, but has been observed elsewhere in databases that incorporate a wider range of bulk rock compositions (e.g., Lanari et al. 2014; Vidal et al. 2006).

Discussion

Fe^{3+} estimates in natural minerals

In the absence of direct measurements of X_{Fe3+} in minerals, petrologists need to use estimates in order to account for Fe^{3+} when conducting phase equilibrium modelling and thermobarometry. Ignoring Fe^{3+} in minerals is the same as making an estimate of $X_{Fe3+} = 0$ (see discussion in appendix III of Hawthorne et al. 2012). Various approaches have been taken to estimate Fe^{3+} in minerals where it has not been measured. Powell (1973) in his programme RECALC built in "guesses" for the X_{Fe3+} content of several minerals including muscovite (=0.85), biotite (=0.15), and chlorite (=0.20). For biotite, Dymek (1983) developed an iterative cation-based normalisation procedure that estimates Fe^{3+}, whilst Li et al. (2020) used an estimation method based on principal components regression.

On the basis of the measurements from West-central Maine presented above, Guidotti et al. (1994) argued that corrections for the effect of Fe^{3+} on EPMA-measured X_{Mg} of biotite and muscovite should be routinely applied to metapelites. Whilst it may be appropriate to use the values provided by Guidotti and Dyar as estimates for Fe^{3+} in certain minerals and settings, the applicability of these estimates to metapelites that equilibrated at different P–T conditions and contrasting oxidation states is unknown. Our database, which incorporates the Guidotti and Dyar data, covers a wider range of P–T conditions and oxidation states. Analysis of the database shows that the type of Fe-oxide present is linked to the X_{Fe3+} in the whole rock and in specific minerals (Table 2). Therefore, it is important to identify the Fe-oxide in an assemblage in order to estimate how much Fe^{3+} may be present before conducting phase equilibrium modelling or thermobarometry.

Fe^{3+} in phase equilibrium modelling

Here we suggest some 'best practices' for incorporating Fe^{3+} as a component in phase equilibrium modelling calculations. First, the proportion of total iron in the bulk composition that is Fe^{3+} must be determined (i.e., whole rock X_{Fe3+}). Whilst, measurement of whole rock X_{Fe3+} by titration is more common than measurement of X_{Fe3+} in minerals, these values should be considered a maximum, due to surface weathering processes or post-crushing, pre-analysis oxidation (Diener and Powell 2010). An alternate or complementary method is for authors to note the identity and modal abundance of the Fe-oxide in their sample. A value of X_{Fe3+} can be estimated by comparison with whole rock X_{Fe3+} analyses from similar rock types with the same oxide assemblage (e.g., using the whole rock database presented here for metapelites). However, as noted above the reliability of this method may be affected by varying modal abundances of silicate minerals that can contain Fe^{3+} (Diener and Powell 2010). Another method is to construct a bulk composition by combining phase proportions with their representative compositions in which Fe^{3+} contents have been estimated (e.g., Forshaw et al. 2019; George et al. 2021; Palin et al. 2016).

We recommend using as many of the above methods as possible to help constrain the whole rock X_{Fe3+}. These measured or estimated whole rock X_{Fe3+} values may then be used as input for phase equilibrium modelling. For a thorough assessment of the effects of varying whole rock X_{Fe3+} on predicted equilibrium assemblage diagrams, we suggest, similarly to Diener and Powell (2010), that P-X_{Fe3+} and T-X_{Fe3+} phase diagrams be calculated. These diagrams can be used to determine the range of whole rock X_{Fe3+} values for which the observed Fe-oxide mineral assemblage is most closely predicted. In addition, matching the predicted X_{Mg} values of silicate minerals to those observed in the sample provides a further constraint on the whole rock X_{Fe3+} (e.g., Doukkari et al. 2018; Schorn and Diener 2019). Adopting these measures helps ensure that the whole rock X_{Fe3+} used for the modelling is consistent with the thermodynamic dataset and solution models chosen.

Of the thermodynamic datasets and solution models currently available, only Holland and Powell (2011; dataset 6.2) and the solution models of White et al. (2014a) incorporate enough Fe^{3+} end members to simulate natural Fe^{3+}-bearing phase equilibria. This dataset broadly predicted the correct Fe-oxide combinations for a variety of whole rock X_{Fe3+}, and the correlation amongst the observed Fe^{3+} contents and X_{Fe3+} values of white mica and biotite with whole rock X_{Fe3+} and the type of Fe-oxide present (Figs. 6, 7, 8, 10). It also correctly predicted the decrease in the number of Fe^{3+} cations in white mica with increasing temperatures (Figs. 4, 8). However, the predicted variations in the X_{Fe3+} of white mica and biotite with pressure and temperature are not observed in the natural database, recognising that the magnitude of these predicted changes may be within the uncertainty of the measured values (Figs. 4, 7, 8). In terms of quantitative estimates, predicted values of Fe^{3+} cations and X_{Fe3+} in biotite, chlorite, and staurolite broadly match those observed in nature, but the predicted number of Fe^{3+} cations and X_{Fe3+} in white mica are below those observed in the database (Fig. 10).

Database of X_{Fe3+} in natural rocks and minerals

An important question for future studies is what new data are needed to improve the natural database presented in this paper? Probably the most significant piece of data missing from many samples in the database is the Fe-oxide present in the assemblage (unknown category in Fig. 3c). Only a half to two-thirds of the whole rock, white mica, and biotite X_{Fe3+} data have a specified Fe-oxide as part of the assemblage (Fig. 3c). In addition, it would be helpful to know the modal abundance of the Fe-oxides and the possible presence of lamellae within these resulting from the solid solutions of ilmenite–hematite and magnetite–ulvöspinel–hercynite (e.g., Ague et al. 2001; Chinner 1960; Dougan 1974; Hounslow and Moore 1967; Okrusch 1969; Rumble 1973). Analysis of our database was only able to delineate four broad categories (no Fe-oxide, Ilm-, Mag-, and Hem-bearing), whereas future analysis might be able to separate rocks further, perhaps allowing for better estimation of Fe^{3+} in rocks and minerals.

In our database, there is a lack of X_{Fe3+} data for chlorite and staurolite. This is probably in part due to the restricted stability range of these minerals in P–T space, and the relatively low measured values of staurolite and chlorite that have been analysed, such that many authors assume Fe^{3+} is negligible. Nevertheless, these minerals may be modally abundant in some metapelites and they have large FeO contents, meaning that even at low X_{Fe3+}, they may contain a non-negligible portion of the Fe^{3+} in the rock.

Another aspect of our database is that it is dominated by analyses of rocks and minerals from samples with relatively low oxidation states. Whilst more oxidised, hematite-bearing schists may not be as common in the geological record, there are many examples of regions world-wide where they occur alongside the more prevalent rocks of lower oxidation state: Barrow's zones, Scotland (Ague et al. 2001; Chinner 1960; Dempster 1983; McNamara 1965); Northern Apennines, Italy (Lo Pò and Braga 2014); New Hampshire, U.S.A. (Rumble 1978, 1973); South Dakota, U.S.A. (Helms and Labotka 1991); New Mexico, U.S.A. (Grambling and Williams 1985; Williams and Grambling 1990); California, U.S.A. (Labotka 1980, 1981); Ontario, Canada (Carmichael et al. 1978; Hounslow and Moore 1967); Anosyen, Madagascar (Boger et al. 2012); and Ryoke, Japan (Hiroi 1983). Finally, the majority of mineral X_{Fe3+} measurements included in the database are bulk analyses, which do not record variation in Fe^{3+} contents at the micrometre scale, such as has been documented in recent XANES studies (e.g., Dyar et al. 2002; Masci et al. 2019; Schmid et al. 2003). Documenting changes in X_{Fe3+} with respect to the textural setting of the minerals, and possible zoning of X_{Fe3+} in minerals, may provide greater insight into the phase relations of these silicates and how Fe^{3+} is distributed amongst minerals in metapelites.

Conclusions

We have collated a database of 591 natural metapelites from 47 localities in which measurements of Fe^{2+} and Fe^{3+} were made for one or more of the rock composition and constituent minerals. There are 785 individual minerals with measured X_{Fe3+}, in decreasing order of abundance: biotite, white mica, chlorite, and staurolite. We compare our observations of the number of Fe^{3+} cations and X_{Fe3+} in these minerals to the predictions of phase equilibrium modelling using dataset 6.2 (Holland and Powell 2011) and the solution models of White et al. (2014a). The main conclusions of this work are:

- Determinations of X_{Fe3+} in minerals using wet chemical, Mössbauer spectroscopy, and XANES spectroscopy techniques are generally consistent.
- Average ($\pm 1\sigma$) X_{Fe3+} values for whole rock, biotite, white mica, chlorite, and staurolite are 0.23 ± 0.16, 0.11 ± 0.08, 0.55 ± 0.18, 0.08 ± 0.07, and 0.06 ± 0.05, respectively.
- The average ($\pm 1\sigma$) number of Fe^{3+} cations in biotite, white mica, chlorite, and staurolite is 0.28 ± 0.19 (22 O + Ti cations pfu), 0.17 ± 0.13 (22O pfu), 0.31 ± 0.27 (28O pfu), and 0.20 ± 0.17 (46O pfu), respectively.
- Mean whole rock X_{Fe3+} is similar for ilmenite- and magnetite-bearing metapelites, as well as those with no Fe-oxide, but is significantly higher for hematite-bearing ones.
- The mean number of Fe^{3+} cations and X_{Fe3+} values in white mica and biotite correlate with the type of Fe-oxide present in the rock, with the highest values in magnetite- and hematite-bearing rocks.
- The mean predicted number of Fe^{3+} cations and X_{Fe3+} in biotite, chlorite, and staurolite broadly match those observed in nature, but for white mica the mean predicted X_{Fe3+} is underestimated by 0.2–0.4 and the number of Fe^{3+} cations by 0.05–0.2.
- Thermodynamically-predicted increases in the number of Fe^{3+} cations and X_{Fe3+} of white mica and biotite with whole rock X_{Fe3+} mirror those observed in nature.
- Thermodynamically-predicted grade- and pressure-related variations of X_{Fe3+} in white mica and biotite are not observed in nature.

Supplementary Information The online version contains supplementary material available at https://doi.org/10.1007/s00410-021-01814-4.

Acknowledgements This research represents a portion of Forshaw's doctoral dissertation at the University of Calgary. We acknowledge the

painstaking work of petrologists in obtaining wet chemical analyses of minerals prior to the widespread use of the electron microprobe, especially those involving measurement of Fe^{2+} and Fe^{3+}. Darby Dyar is thanked for providing unpublished data for the West-central Maine region. Benoît Dubacq and Johann Diener are thanked for their insightful and constructive reviews, and Daniela Rubatto for her editorial handling.

Funding Funding for this work was provided by a Natural Sciences and Engineering Research Council of Canada Discovery Grant (037233) to D.R.M. Pattison.

Availability of data and materials Not applicable.

Code availability Not applicable.

Declarations

Conflict of interest Not applicable.

References

Ague JJ (1991) Evidence for major mass transfer and volume strain during regional metamorphism of pelites. Geology 19:855–858. https://doi.org/10.1130/0091-7613(1991)019<0855:EFMMTA>2.3.CO;2

Ague JJ, Baxter EF, Eckert JO (2001) High f_{O2} during sillimanite zone metamorphism of part of the Barrovian type locality, Glen Clova, Scotland. J Petrol 42:1301–1320. https://doi.org/10.1093/petrology/42.7.1301

Albee AL (1965) Phase equilibria in three assemblages of kyanite-zone pelitic schists, Lincoln Mountain quadrangle, central Vermont. J Petrol 6:246–301. https://doi.org/10.1093/petrology/6.2.246

Atherton MP (1968) The variation in garnet, biotite and chlorite composition in medium grade pelitic rocks from the Dalradian, Scotland, with particular reference to the zonation in garnet. Contrib Mineral Petrol 18:347–371. https://doi.org/10.1007/BF00399696

Atherton MP, Brotherton MS (1982) Major element composition of the pelites of the Scottish Dalradian. Geol J 17:185–221. https://doi.org/10.1002/gj.3350170303

Bajt S, Sutton SR, Delaney JS (1994) X-ray microprobe analysis of iron oxidation states in silicates and oxides using X-ray absorption near edge structure (XANES). Geochim Cosmochim Acta 58:5209–5214. https://doi.org/10.1016/0016-7037(94)90305-0

Bancroft GM, Brown JR (1975) A Mössbauer study of coexisting hornblendes and biotites: ratios quantitative Fe^{3+}/Fe^{2+}. Am Mineral 60:265–272

Banno S (1964) Petrologic studies on Sanbagawa crsystalline schists in the Bessi-ino District, Central Sikoku, Japan. J Fac Sci Univ Tokyo Sec 2 15:203–319

Barker F (1962) Cordierite-garnet gneiss and associated microcline-rich pegmatite at Sturbridge, Massachusetts and Union, Connecticut. Am Mineral 47:907–918

Barth TFW (1936) Structural and petrologic studies in Dutchess County, New York: Part II. Petrology and metamorphism of the Paleozoic rocks. Bull Geol Soc Am 47:775–850. https://doi.org/10.1130/GSAB-47-775

Berman RG (1988) Internally-consistent thermodynamic data for minerals in the system Na_2O-K_2O-CaO-MgO- FeO-Fe_2O_3-Al_2O_3-SiO_2-TiO_2-H_2O-CO_2. J Petrol 29:445–522.

Best MG, Weiss LE (1964) Mineralogical relations in some pelitic hornfelses from the southern Sierra Nevada, California. Am Mineral 49:1240–1266

Blackburn WH (1967) The spatial degree of chemical equilibrium in some high grade metamorphic rocks. Doctoral thesis, Massachusetts Institute of Technology

Boger SD, White RW, Schulte B (2012) The importance of iron speciation (Fe^{+2}/Fe^{+3}) in determining mineral assemblages: an example from the high-grade aluminous metapelites of southeastern Madagascar. J Metamorph Geol 30:997–1018. https://doi.org/10.1111/jmg.12001

Butler BCM (1965) A chemical study of some rocks of the Moine Series of Scotland. Q J Geol Soc 121:163–208. https://doi.org/10.1144/gsjgs.121.1.0163

Butler BCM (1967) Chemical Study of Minerals from the Moine Schists of the Ardnamurchan Area, Argyllshire, Scotland. J Petrol 8:233–267. https://doi.org/10.1093/petrology/8.2.233

Card KD (1964) Metamorphism in the Agnew Lake Area, Sudbury District, Ontario, Canada. Geol Soc Am Bull 75:1011–1030. https://doi.org/10.1130/0016-7606(1964)75[1011:MITALA]2.0.CO;2

Carmichael DM, Moore JM, Skippen GB (1978) Isograds around the Hastings metamorphic "low,". In: Mackasey AL, Currie WO (eds) Toronto '78 Field Trips Guidebook—Geological Association of Canada–Geological Association of America Combined Meeting, pp 325–346

Cesare B, Cruciani G, Russo U (2003) Hydrogen deficiency in Ti-rich biotite from anatectic metapelites (El Joyazo, SE Spain): Crystal-chemical aspects and implications for high-temperature petrogenesis. Am Mineral 88:583–595. https://doi.org/10.2138/am-2003-0412

Cesare B, Meli S, Nodari L, Russo U (2005) Fe^{3+} reduction during biotite melting in graphitic metapelites: another origin of CO2 in granulites. Contrib Mineral Petrol 149:129–140. https://doi.org/10.1007/s00410-004-0646-3

Chakraborty KR, Sen SK (1967) Regional metamorphism of pelitic rocks around Kandra, Singhbhum, Bihar. Contrib Mineral Petrol 16:210–232. https://doi.org/10.1007/BF00371093

Chinner GA (1960) Pelitic gneisses with varying ferrous/ferric ratios from Glen Clova, Angus, Scotland. J Petrol 1:178–217. https://doi.org/10.1093/petrology/1.1.178

Chinner GA (1962) Almandine in thermal aureoles. J Petrol 3:316–341. https://doi.org/10.1093/petrology/3.3.316

Chinner GA (1965) The kyanite isograd in Glen Clova, Angus, Scotland. Mineral Mag 34:132–143. https://doi.org/10.1180/minmag.1965.034.268.11

Coggon R, Holland TJB (2002) Mixing properties of phengitic micas and revised garnet-phengite thermobarometers. J Metamorph Geol 20:683–696. https://doi.org/10.1046/j.1525-1314.2002.00395.x

Crameri F (2021) Scientific colour maps. https://doi.org/10.5281/zenodo.4491293

Crameri F, Shephard GE, Heron PJ (2020) The misuse of colour in science communication. Nat Commun 11:1–10. https://doi.org/10.1038/s41467-020-19160-7

Dallmeyer RD (1974) Metamorphic history of the Northeastern Reading Prong, New York and Northern New Jersey. J Petrol 15:325–359. https://doi.org/10.1093/petrology/15.2.325

Das BK (1973) Petrochemical study of pelitic schists and coexisting minerals of lower Kumaon Himalaya. Neues Jahrb Für Mineral Monatshefte 12:547–563

De Capitani C, Brown TH (1987) The computation of chemical equilibrium in complex systems containing non-ideal solutions. Geochim Cosmochim Acta 51:2639–2652. https://doi.org/10.1016/0016-7037(87)90145-1

De Capitani C, Petrakakis K (2010) The computation of equilibrium assemblage diagrams with Theriak/Domino software. Am Mineral 95:1006–1016. https://doi.org/10.2138/am.2010.3354

Deer WA, Howie RA, Zussman J (2013) An introduction to the rock-forming minerals, 3rd edn. Longman Group Limited. https://doi.org/10.1180/DHZ

Delaney JS, Bajt S, Sutton SR, Dyar MD (1996) In situ microanalysis of $Fe^{3+}/\Sigma Fe$ ratios in amphibole by X-ray Absorption near edge structure (XANES) spectroscopy. Geochem Soc Spec Publ 5. pp 170–177

Delaney JS, Dyar MD, Steven SR, Bajt S (1998) Redox ratios with relevant resolution: solving an old problem by using the synchrotron microXANES probe. Geology 26:139–142. https://doi.org/10.1130/0091-7613(1998)026%3c0139:RRWRRS%3e2.3.CO;2

Dempster TJ (1983) Studies of orogenic evolution in the Scottish Dalradian. Doctoral thesis, University of Edinburgh

Diener JFA, Powell R (2010) Influence of ferric iron on the stability of mineral assemblages. J Metamorph Geol 28:599–613. https://doi.org/10.1111/j.1525-1314.2010.00880.x

Dodge FCW, Smith VC, Mays RE (1969) Biotites from granitic rocks of the Central Sierra Nevada Batholith, California. J Petrol 10:250–271. https://doi.org/10.1093/petrology/10.2.250

Dougan TW (1974) Cordierite gneisses and associated lithologies of the Guri area, Northwest Guayana Shield, Venezuela. Contrib Mineral Petrol 46:169–188. https://doi.org/10.1007/BF00487554

Doukkari SA, Diener JFA, Ouzegane K, Kienast J-R (2018) Mineral equilibrium modelling and calculated chemical potential relations of reaction textures in the ultrahigh-temperature In Ouzzal terrane (In Hihaou area, Western Hoggar, Algeria). J Metamorph Geol. https://doi.org/10.1111/jmg.12441

Droop GTR (1987) A general equation for estimating Fe^{3+} concentrations in ferromagnesian silicates and oxides from microprobe analyses, using stoichiometric criteria. Mineral Mag 51:431–435. https://doi.org/10.1180/minmag.1987.051.361.10

Dyar MD (1990) Mössbauer spectra of biotite from metapelites. Am Mineral 75:656–666

Dyar MD (1993) Mössbauer spectroscopy of tetrahedral Fe^{3+} in trioctahedral micas. Discussion 78:669–671

Dyar MD, Burns RB (1986) Mössbauer spectral study of ferruginous one-layer trioctahedral micas. Am Mineral 71:955–965

Dyar MD, Perry CL, Rebbert CR, Dutrow BL, Holdaway MJ, Lang HM (1991) Mössbauer spectroscopy of synthetic and naturally occurring staurolite. Am Mineral 76:27–41

Dyar MD, Guidotti CV, Holdaway MJ, Colucci M (1993a) Non-stoichiometric hydrogen contents in common rock-forming hydroxyl silicates. Geochim Cosmochim Acta 57:2913–2918. https://doi.org/10.1016/0016-7037(93)90399-H

Dyar MD, Mackwell SJ, McGuire AV, Cross LR, Robertson JD (1993b) Crystal chemistry of Fe^{3+} and H^+ in mantle kaersutite: implications for mantle metasomatism. Am Mineral 78:968–979

Dyar MD, Delaney JS, Sutton SR (2001) Fe XANES spectra of iron-rich micas. Eur J Mineral 13:1079–1098. https://doi.org/10.1127/0935-1221/2001/0013-1079

Dyar MD, Lowe EW, Guidotti CV, Delaney JS (2002) Fe^{3+} and Fe^{2+} partitioning among silicates in metapelites: a synchrotron micro-XANES study. Am Mineral 87:514–522. https://doi.org/10.2138/am-2002-0414

Dyar MD, Breves EA, Emerson E, Bell SW, Nelms M, Ozanne MV, Peel SE, Carmosino ML, Tucker JM, Gunter ME, Delaney JS, Lanzirotti A, Woodland AB (2012) Accurate determination of ferric iron in garnets by bulk Mössbauer spectroscopy and synchrotron micro-XANES. Am Mineral 97:1726–1740. https://doi.org/10.2138/am.2012.4107

Dymek RF (1983) Titanium, aluminum and interlayer cation substitutions in biotite from high-grade gneisses, West Greenland. Am Mineral 68:880–899

Eckert JOJ (1988) Petrology and tectonic implications of the transition from the staurolite-kyanite zone to the Wayah granulite-facies metamorphic core, southwest North Carolina Blue Ridge; including quantitative analysis of mineral homogeneity. Doctoral thesis, Texas A&M University

Ernst WG, Wai CM (1970) Mössbauer, infrared, X-ray and optical study of cation ordering and dehydrogenation in natural and heat-treated sodic amphiboles. Am Mineral 55:1226–1258

Eugster HP, Wones DR (1962) Stability relations of the ferruginous biotite, annite. J Petrol 3:82–125. https://doi.org/10.1093/petrology/3.1.82

Evans KA, Dyar MD, Reddy SM, Lanzirotti A, Adams DT, Tailby N (2014) Variation in XANES in biotite as a function of orientation, crystal composition, and metamorphic history. Am Mineral 99:443–457. https://doi.org/10.1515/am.2014.4222

Fleming PD (1971) Metamorphism and folding in the Mt. Lofty Ranges, South Australia, with particular reference to the Dawesley-Kanmantoo area. Doctoral thesis, University of Adelaide

Fleming PD (1972) Mg-Fe distribution between coexisting garnet and biotite, and the status of fibrolite in the andalusite-staurolite zone of the Mt Lofty Ranges, South Australia. Geol Mag 109:477–482. https://doi.org/10.1017/S0016756800042758

Flinn D (1967) The metamorphic rocks of the southern part of the Mainland of Shetland. Geol J 5:251–290. https://doi.org/10.1002/gj.3350050203

Forshaw JB, Waters DJ, Pattison DRM, Palin RM, Gopon P (2019) A comparison of observed and thermodynamically predicted phase equilibria and mineral compositions in mafic granulites. J Metamorph Geol 37:153–179. https://doi.org/10.1111/jmg.12454

Foster MD (1960) Interpretation of the composition of trioctahedral micas. US Geol Surv Prof Pap 354-B:11–48

Foster MD (1962) Interpretation of the composition and a classification of the chlorites. US Geol Surv Prof Pap 414-A:1–33

Foster MD (1964) Water content of micas and chlorites. US Geol Surv Prof Pap 474-F:1–15

Fritz SF, Popp RK (1985) A single-dissolution technique for determining FeO and Fe_2O_3 in rock and mineral samples. Am Mineral 70:961–968

Geiger CA, Armbruster T, Khomenko V, Quartieri S (2000a) Cordierite I: the coordination of Fe^{2+}. Am Mineral 85:1255–1264. https://doi.org/10.2138/am-2000-8-918

Geiger CA, Rager H, Czank M (2000b) Cordierite III: the site occupation and concentration of Fe^{3+}. Contrib Mineral Petrol 140:344–352. https://doi.org/10.1007/s004100000194

George FR, Waters DJ, Gough SJ, Searle MP, Forshaw JB (2021) Phase equilibria and microstructural constraints on the high temperature building of the Kohistan island arc: the Jijal garnet granulites, northern Pakistan. Metamorph Geol. https://doi.org/10.1111/jmg.12622

Goossens PJ (1970) Le comportement des grenats dans les séries métamorphiques de Zermatt (Suisse). Schweizerische Mineral Petrogr Mitteilungen 50:291–320. https://doi.org/10.5169/seals-39259

Grambling JA, Williams ML (1985) The effects of Fe^{3+} and Mn^{3+} on aluminum silicate phase relations in north-central New Mexico, U.S.A. J Petrol 26:324–354. https://doi.org/10.1093/petrology/26.2.324

Green JC (1963) High-level metamorphism of pelitic rocks in Northern New Hampshire. Am Mineral 48:991–1023

Guidotti CV, Dyar MD (1991) Ferric iron in metamorphic biotite and its petrologic and crystallochemical implications. Am Mineral 76:161–175

Guidotti CV, Sassi FP (1998a) Miscellaneous isomorphous substitutions in Na-K white micas: a review, with special emphasis to metamorphic micas. Rend Lincei 53:1689–1699. https://doi.org/10.1017/CBO9781107415324.004

Guidotti CV, Sassi FP (1998b) Petrogenetic significance of Na-K white mica mineralogy: recent advances for metamorphic rocks. Eur J Mineral 10:815–854. https://doi.org/10.1127/ejm/10/5/0815

Guidotti CV, Yates MG, Dyar MD, Taylor ME (1994) Petrogenetic implications of the Fe^{3+} content of muscovite in pelitic schists. Am Mineral 79:793–795

Hall DJ (1970) Compositional variations in biotites and garnets from kyanite and sillimanite zone mica schists, Orange Area, Massachusetts and New Hampshire. University of Massachusetts

Hansen JW (1972) Zur Geologie, Petrographie und Geochemie der Bündnerschiefer-Serien zwischen Nufenenpass (Schweiz) und Cascata Toce (Italia). Schweizerische Mineral Petrogr Mitteilungen 52:109–153. https://doi.org/10.5169/seals-40600

Hattori H (1967) Occurrence of sillimanite-garnet-biotite gneisses and their significance in metamorphic zoning in the South Island, New Zealand. New Zeal J Geol Geophys 10:269–299. https://doi.org/10.1080/00288306.1967.10428197

Hawthorne FC, Ungaretti L, Oberti R, Caucia F, Callegari A (1993) The crystal chemistry of staurolite. llI. Local order and chemical composition. Can Mineral 31:597–616

Hawthorne FC, Oberti R, Harlow GE, Maresch WV, Martin RF, Schumacher JC, Welch MD (2012) IMA report: Nomenclature of the amphibole supergroup. Am Mineral 97:2031–2048. https://doi.org/10.2138/am.2012.4276

Hayama Y (1964) Progressive metamorphism of pelitic and psammitic rocks in the Komagane district, Nagano Pref., Central Japan. J Fac Sci Univ Tokyo Sec 2 15:321–369

Helms TS, Labotka TC (1991) Petrogenesis of early Proterozoic pelitic schists of the southern Black Hills, South Dakota: constraints on regional low-pressure metamorphism. Geol Soc Am Bull 103:1324–1334. https://doi.org/10.1130/0016-7606(1991)103%3c1324:POEPPS%3e2.3.CO;2

Hietanen A (1967) On the facies series in various types of metamorphism. J Geol 75:187–214. https://doi.org/10.1086/627246

Hietanen A (1969) Distribution of Fe and Mg between garnet, staurolite and biotite in aluminum-rich schist in various metamorphic zones north of the Idaho Batholith. Am J Sci 267:422–456. https://doi.org/10.2475/ajs.267.3.422

Hiroi Y (1983) Progressive metamorphism of the Unazuki pelitic schists in the Hida terrane, central Japan. Contrib Mineral Petrol 82:334–350. https://doi.org/10.1007/BF00399711

Höfer HE, Brey GP, Schulz-Dobrick B, Oberhänsli R (1994) The determination of the oxidation state of iron by the electron microprobe. Eur J Mineral 6:407–418. https://doi.org/10.1127/ejm/6/3/0407

Holdaway MJ, Mukhopadhyay B, Dyar MD, Guidotti CV, Dutrow BL (1997) Garnet-biotite geothermometry revised: new Margules parameters and a natural specimen data set from Maine. Am Mineral 82:582–595

Holland TJB, Blundy JD (1994) Non-ideal interactions in calcic amphiboles and their bearing on amphibole-plagioclase thermometry. Contrib Mineral Petrol 116:433–447. https://doi.org/10.1007/BF00310910

Holland TJB, Powell R (1990) An enlarged and updated internally consistent thermodynamic dataset with uncertainties and correlations: the system K_2O–Na_2O–CaO–MgO–MnO–FeO–Fe_2O_3–Al_2O_3–TiO_2–SiO_2–C–H_2O–O_2. J Metamorph Geol 8:89–124. https://doi.org/10.1111/j.1525-1314.1990.tb00458.x

Holland TJB, Powell R (1998) An internally consistent thermodynamic data set for phases of petrological interest. J Metamorph Geol 16:309–343. https://doi.org/10.1111/j.1525-1314.1998.00140.x

Holland TJB, Powell R (2003) Activity-composition relations for phases in petrological calculations: an asymmetric multicomponent formulation. Contrib Mineral Petrol 145:492–501. https://doi.org/10.1007/s00410-003-0464-z

Holland TJB, Powell R (2011) An improved and extended internally consistent thermodynamic dataset for phases of petrological interest, involving a new equation of state for solids. J Metamorph Geol 29:333–383. https://doi.org/10.1111/j.1525-1314.2010.00923.x

Hounslow AW, Moore JM (1967) Chemical petrology of Grenville schists near Fernleigh. Ontario J Petrol 8:1–28. https://doi.org/10.1093/petrology/8.1.1

Hunziker JCV (1966) Zur Geologie und Geochemie des Gebietes zwischen Valle Antigorio (Provincia di Novara) und Valle di Campo (Kt. Tessin). Schweizerische Mineral Petrogr Mitteilungen 46:473–552. https://doi.org/10.5169/seals-36138

Joyce AS (1970) Chemical variation in a pelitic hornfels. Chem Geol 6:51–58. https://doi.org/10.1016/0009-2541(70)90005-7

Kamineni DC (1975) Chemical mineralogy of some cordierite-bearing rocks near Yellowknife, Northwest Territories, Canada. Contrib Mineral Petrol 53:293–310. https://doi.org/10.1007/BF00382445

Kretz R (1990) Biotite and garnet compositional variation and mineral equilibria in Grenville gneisses of the Otter Lake area, Quebec. J Metamorph Geol 8:493–506. https://doi.org/10.1111/j.1525-1314.1990.tb00482.x

Kutsukake T (1976) Distribution of major and some distribution of major and minor elements in pelitic metamorphic rocks in the Ryôke Zone of Central Japan, in comparison with the non-metamorphic 'Palaeozoic' Shales. Mem Fac Sci Kyoto Univ Ser Geol Mineral 42:107–129

Kutsukake T (1977) Petrological studies on the Ryoke metamorphic rocks in the Toyone-mura Area, Aichi Prefecture, Japan. Mem Fac Sci Kyoto Univ Ser Geol Miner XLIII:49–110

Kwak TAP (1968) Metamorphic petrology and geochemistry across the Grenville Province - Southern Province Boundary Dill Township, Sudbury, Ontario. Doctoral thesis, McMaster University

Labotka TC (1980) Petrology of a medium-pressure regional metamorphic terrane, Funeral Mountains, California. Am Mineral 65:670–689

Labotka TC (1981) Petrology of an andalusite-type regional metamorphic terrane, Panamint mountains, California. J Petrol 22:261–296. https://doi.org/10.1093/petrology/22.2.261

Lal RK, Moorhouse WW (1969) Cordierite–gedrite rocks and associated gneisses of Fishtail Lake, Harcourt Township, Ontario. Can J Earth Sci 6:145–165. https://doi.org/10.1139/e69-014

Lal RK, Shukla RS (1975) Low-pressure regional metamorphism in the northern portion of the Khetri Copper Belt of Rajasthan, India. Neues Jahrb Für Mineral Abhandlungen 124:294–325

Lalonde AE, Rancourt DG, Ping JY (1998) Accuracy of ferric/ferrous determinations in micas: a comparison of Mössbauer spectroscopy and the Pratt and Wilson wet-chemical methods. Hyperfine Interact 117:175–204. https://doi.org/10.1023/A:1012607813487

Lambert RSJ (1959) The mineralogy and metamorphism of the Moine Schists of the Morar and Knoydart Districts of Inverness-shire. Trans Edinburgh Geol Soc 63:553–588. https://doi.org/10.1017/S0080456800003148

Lanari P, Wagner T, Vidal O (2014) A thermodynamic model for di-trioctahedral chlorite from experimental and natural data in the system MgO-FeO-Al_2O_3-SiO_2-H_2O: applications to P-T sections

and geothermometry. Contrib Mineral Petrol 167:1–19. https://doi.org/10.1007/s00410-014-0968-8
Leake BE (1958) Composition of pelites from Connemara, Co., Galway, Ireland. Geol Mag 95:281–296. https://doi.org/10.1017/S0016756800062841
Lempart M, Derkowski A, Luberda-Durnas K, Skiba M, Błachowski A (2018) Dehydrogenation and dehydroxylation as drivers of the thermal decomposition of Fe-chlorites. Am Mineral 103:1837–1850. https://doi.org/10.2138/am-2018-6541
Lempart M, Derkowski A, StrÄczek T, Kapusta C (2020) Systematics of H_2 and H_2O evolved from chlorites during oxidative dehydrogenation. Am Mineral 105:932–944. https://doi.org/10.2138/am-2020-7326
Li X, Zhang C, Almeev RR, Zhang XC, Zhao XF, Wang LX, Koepke J, Holtz F (2019) Electron probe microanalysis of $Fe^{2+}/\Sigma Fe$ ratios in calcic and sodic-calcic amphibole and biotite using the flank method. Chem Geol 509:152–162. https://doi.org/10.1016/j.chemgeo.2019.01.009
Li X, Zhang C, Behrens H, Holtz F (2020) Calculating biotite formula from electron microprobe analysis data using a machine learning method based on principal components regression. Lithos 356–357:105371. https://doi.org/10.1016/j.lithos.2020.105371
Lo Pò D, Braga R (2014) Influence of ferric iron on phase equilibria in greenschist facies assemblages: The hematite-rich metasedimentary rocks from the Monti Pisani (Northern Apennines). J Metamorph Geol 32:371–387. https://doi.org/10.1111/jmg.12076
Lundgren LW (1966) Muscovite reactions and partial melting in Southeastern Connecticut. J Petrol 7:421–453. https://doi.org/10.1093/petrology/7.3.421
Lyons JB, Morse SA (1970) Mg/Fe partitioning in garnet and biotite from some granitic, pelitic, and calcic rocks. Am Mineral 55:231
Masci L, Dubacq B, Verlaguet A, Chopin C, Andrade VD, Herviou C (2019) A XANES and EPMA study of Fe^{3+} in chlorite: Importance of oxychlorite and implications for cation site distribution and thermobarometry. Am Mineral 104:403–417. https://doi.org/10.2138/am-2019-6766
Mason B (1962) Metamorphism in the Southern Alps of New Zealand. Bull Am Museum Nat Hist 123:4
Mather JD (1970) The biotite isograd and the lower greenschist facies in the Dalradian rocks of Scotland. J Petrol 11:253–275. https://doi.org/10.1093/petrology/11.2.253
McKay DS (1964) Chemistry of coexisting metamorphic muscovite and biotite from eastern New York and western Connecticut. Doctoral thesis, Rice University
McNamara MJ (1965) The lower greenschist facies in the Scottish Highlands. Geol Foren Istockholm Forh 87:347–389. https://doi.org/10.1080/11035896509448918
Mielke H, Blümel P, Langer K (1979) Regional low-pressure metamorphism of low and medium grade in metapelites and -psammites of the Fichtelgebirge area, NE-Bavaria. Neues Jahrb Für Mineral Abhandlungen 137:83–112
Miyashiro A (1956) Data on garnet-biotite equilibria in some metamorphic rocks of the Ryoke zone. J Geol Soc Japan 62:700–702
Miyashiro A (1958) Regional metamorphism of the Gosaisyo-Takanuki District in the Central Abukuma Plateau. J Fac Sci Univ Tokyo Sect II 11:220–271
Miyashiro A (1961) Evolution of metamorphic belts. J Petrol 2:277–311. https://doi.org/10.1093/petrology/2.3.277
Moeller KJ (1991) The crystal chemistry of chlorite in metapelites as found in the Rangeley area, W. Maine. Masters thesis, University of Oregon
Mohr DW, Newton RC (1983) Kyanite-staurolite metamorphism in sulfidic schists of the Anakeesta formation, Great Smoky mountains, North Carolina. Am J Sci 283:97–134. https://doi.org/10.2475/ajs.283.2.97
Moore JM (1960) Phase relations in the contact aureole of the Onawa pluton, Maine. Doctoral thesis, Massachusetts Institute of Technology
Okrusch M (1969) Die Gneishornfelse um Steinach in der Oberpfalz. Contrib Mineral Petrol 22:32–72. https://doi.org/10.1007/BF00388012
Okrusch M (1971) Garnet-cordierite-biotite equilibria in the Steinach aureole, Bavaria. Contrib Mineral Petrol 32:1–23. https://doi.org/10.1007/BF00372230
Ono A (1969) Zoning of the metamorphic rocks in the Takato-Sioziri area, Nagano Prefecture. J Geol Soc Jpn 10:521–536
Palin RM, Weller OM, Waters DJ, Dyck B (2016) Quantifying geological uncertainty in metamorphic phase equilibria modelling; a Monte Carlo assessment and implications for tectonic interpretations. Geosci Front 7:591–607. https://doi.org/10.1016/j.gsf.2015.08.005
Pattison DRM, Tracy RJ (1991) Phase equilibria and thermobarometry of metapelites. Rev Mineral Geochem 26:106–206
Phinney WC (1963) Phase equilibria in the metamorphic rocks of St. Paul Island and Cape North, Nova Scotia. J Petrol 4:90–130. https://doi.org/10.1093/petrology/4.1.90
Powell R (1973) Mineral equilibria in the Leven schists near Fort William, Inverness-shire. Doctoral thesis, University of Oxford
Pratt JH (1894) On the determinations of ferrous iron in silicates. Am J Sci 48:149
Rancourt DG (1993) Mössbauer spectroscopy of tetrahedral Fe^{3+} in trioctahedral micas. Reply. Am Mineral 78:669–671
Rancourt DG, Dang MZ, Lalonde AE (1992) Mössbauer spectroscopy of tetrahedral Fe^{3+} in trioctahedral micas. Am Mineral 77:34–43
Redhammer GJ, Beran A, Dachs E, Amthauer G (1993) A Mössbauer and X-ray diffraction study of annites synthesized at different oxygen fugacities and crystal chemical implications. Phys Chem Miner 20:382–394. https://doi.org/10.1007/BF00203107
Reinhardt EW (1968) Phase relations in cordierite-bearing gneisses from the Gananoque area, Ontario. Can J Earth Sci 5:455–482. https://doi.org/10.1139/e68-043
Righter K, Dyar MD, Delaney JS, Vennemann TW, Hervig RL, King PL (2002) Correlations of octahedral cations with OH^-, O^{2-}, Cl^-, and F^- in biotite from volcanic rocks and xenoliths. Am Mineral 87:142–153. https://doi.org/10.2138/am-2002-0115
Robinson P, Spear FS, Schumacher JC, Laird J, Klein C, Evans BW, Doolan BL (1982) Phase relations of metamorphic amphiboles: Natural occurrence and theory. In: Veblen DR, Ribbe PH (eds) Reviews in Mineralogy, vol 9B. Amphiboles: Petrology and Experimental Phase Relations, pp 1–211
Rumble D (1973) Fe-Ti oxide minerals from regionally metamorphosed quartzites of western New Hampshire. Contrib Mineral Petrol 42:181–195. https://doi.org/10.1007/BF00371584
Rumble D (1978) Mineralogy, petrology, and oxygen isotopic geochemistry of the Clough Formation, Black Mountain, Western New Hampshire, U.S.A. J Petrol 19:317–340. https://doi.org/10.1093/petrology/19.2.317
Saxena SK (1966) Distribution of elements between coexisting muscovite and biotite and crystal chemical role of titanium in the micas. Neues Jahrb Für Mineral Abhandlungen 105:1–17
Schmid R, Wilke M, Oberhánsli R, Janssens K, Falkenberg G, Franz L, Gaab A (2003) Micro-XANES determination of ferric iron and its application in thermobarometry. Lithos 70:381–392. https://doi.org/10.1016/S0024-4937(03)00107-5
Schorn S, Diener JFA (2019) Seemingly disparate temperatures recorded in coexisting granulite facies lithologies. J Metamorph Geol 37:1049–1078. https://doi.org/10.1111/jmg.12500
Schumacher JC (1991) Empirical ferric iron corrections: necessity, assumptions, and effects on selected geothermobarometers. Mineral Mag 55:3–18. https://doi.org/10.1180/minmag.1991.055.378.02

Schumacher JC (2007) Metamorphic amphiboles: composition and coexistence. Rev Mineral Geochem 67:359–416

Schwander H, Hunziker J, Stern W (1968) Zur Mineralchemie von Hellglimmern in den Tessineralpen. Schweizerische Mineral Petrogr Mitteilungen 48:357–390. https://doi.org/10.5169/seals-37773

Schwarcz HP (1966) Chemical and mineralogic variations in an arkosic quartzite during progressive regional metamorphism. Bull Geol Soc Am 77:509–532. https://doi.org/10.1130/0016-7606(1966)77[509:CAMVIA]2.0.CO;2

Sen SK, Chakraborty KR (1968) Magnesium-iron exchange equilibrium in garnet-biotite and metamorphic grade. Neues Jahrb Für Mineral Abhandlungen 108:181–207

Senior A, Leake BE (1978) Regional metasomatism and the geochemistry of the Dalradian metasediments of Connemara, Western Ireland. J Petrol 19:585–625. https://doi.org/10.1093/petrology/19.3.585

Shapiro L, Brannock WW (1956) Rapid analysis of silicate rocks. Geol Surv Bull US Gov Print Off 1036

Sharma RS, Narayan V (1975a) Distribution of elements between coexisting garnet-biotite and muscovite-biotite pairs from polymetamorphic schists of south-east Beawar, Rajasthan, India. Schweizerische Mineral Petrogr Mitteilungen 55:61–77. https://doi.org/10.5169/seals-43065

Sharma RS, Narayan V (1975b) Petrology of polymetamorphic schists from an Archaean complex terrain, southeast of Beawar, Rajasthan, India. Neues Jahrb Für Mineral Abhandlungen 124:190–222

Shaw D (1956) Geochemistry of pelitic rocks. Part III: major elements and general geochemistry. Bull Geol Soc Am 67:919–934. https://doi.org/10.1130/0016-7606(1956)67[919:GOPRPI]2.0.CO;2

Snelling NJ (1957) Notes on the petrology and mineralogy of the barrovian metamorphic zones. Geol Mag 94:297–304. https://doi.org/10.1017/S0016756800068734

Stephenson NCN (1979) Coexisting garnets and biotites from Precambrian gneisses of the south coast of Western Australia. Lithos 6:74–87. https://doi.org/10.1016/0024-4937(79)90039-2

Stout JH (1972) Phase petrology and mineral chemistry of coexisting amphiboles from Telemark, Norway. J Petrol 13:99–145. https://doi.org/10.1093/petrology/13.1.99

Tajčmanová L, Connolly JAD, Cesare B (2009) A thermodynamic model for titanium and ferric iron solution in biotite. J Metamorph Geol 27:153–165. https://doi.org/10.1111/j.1525-1314.2009.00812.x

Tischendorf G, Förster H-J, Gottesmann B, Rieder M (2007) True and brittle micas: composition and solid-solution series. Mineral Mag 71:285–320. https://doi.org/10.1180/minmag.2007.071.3.285

Vallance TG (1960) Notes on metamorphic and plutonic rocks and their biotites from the Wantabadgery-Adelong-Tumbarumba district, NSW. Linn. Soc. New South Wales

Vidal O, Parra T, Vieillard P (2005) Thermodynamic properties of the Tschermak solid solution in Fe-chlorite: application to natural examples and possible role of oxidation. Am Mineral 90:347–358. https://doi.org/10.2138/am.2005.1554

Vidal O, De Andrade V, Lewin E, Munoz M, Parra T, Pascarelli S (2006) P-T-deformation-Fe^{3+}/Fe^{2+} mapping at the thin section scale and comparison with XANES mapping: application to a garnet-bearing metapelite from the Sambagawa metamorphic belt (Japan). J Metamorph Geol 24:669–683. https://doi.org/10.1111/j.1525-1314.2006.00661.x

Vieillard P (1994) Prediction of enthalpy of formation based on refined crystal structures of multisite compounds: Part 2. application to minerals belonging to the system Li_2O-Na_2O-K_2O-BeO-MgO-CaO-MnO-FeO-Fe_2O_3-Al_2O_3-SiO_2-H_2O. Results and discussion. Geochim Cosmochim Acta. https://doi.org/10.1016/0016-7037(94)90267-4

Walshe JL (1986) A six-component chlorite solid solution model and the conditions of chlorite formation in hydrothermal and geothermal systems. Econ Geol 81:681–703. https://doi.org/10.2113/gsecongeo.81.3.681

Waters DJ, Charnley NR (2002) Local equilibrium in polymetamorphic gneiss and the titanium substitution in biotite. Am Mineral 87:383–396. https://doi.org/10.2138/am-2002-0402

Wenk VE, Schwander H, Hunziker J, Stern W (1963) Zur Mineralchemie von Biotit in den Tessineralpen. Schweizerische Mineral Petrogr Mitteilungen 43:435–463. https://doi.org/10.5169/seals-33463

Wetzel R (1973) Chemismus und physikalische Parameter einiger Chlorite aus der Grünschieferfazies. Schweizerische Mineral Petrogr Mitteilungen 53:273–298. https://doi.org/10.5169/seals-41386

Whipple ER (1974) Quantitative Mössbauer spectra and chemistry of iron. Doctoral thesis, Massachusetts Institute of Technology

White RW, Powell R, Holland TJB, Worley BA (2000) The effect of TiO_2 and Fe_2O_3 on metapelitic assemblages at greenschist and amphibolite facies conditions: mineral equilibria calculations in the system K_2O-FeO-MgO-Al_2O_3-SiO_2-H_2O-TiO_2-Fe_2O_3. J Metamorph Geol 18:497–511. https://doi.org/10.1046/j.1525-1314.2000.00269.x

White RW, Powell R, Clarke GL (2002) The interpretation of reaction textures in Fe-rich metapelitic granulites of the Musgrave Block, Central Australia: Constraints from mineral equilibria calculations in the system. J Metamorph Geol 20:41–55. https://doi.org/10.1046/j.0263-4929.2001.00349.x

White RW, Pomroy NE, Powell R (2005) An in situ metatexite-diatexite transition in upper amphibolite facies rocks from Broken Hill. Australia J Metamorph Geol 23:579–602. https://doi.org/10.1111/j.1525-1314.2005.00597.x

White RW, Powell R, Holland TJB (2007) Progress relating to calculation of partial melting equilibria for metapelites. J Metamorph Geol 25:511–527. https://doi.org/10.1111/j.1525-1314.2007.00711.x

White RW, Powell R, Holland TJB, Johnson TE, Green ECR (2014a) New mineral activity-composition relations for thermodynamic calculations in metapelitic systems. J Metamorph Geol 32:261–286. https://doi.org/10.1111/jmg.12071

White RW, Powell R, Johnson TE (2014b) The effect of Mn on mineral stability in metapelites revisited: new a-x relations for manganese-bearing minerals. J Metamorph Geol 32:809–828. https://doi.org/10.1111/jmg.12095

Whitney DL, Evans BW (2010) Abbreviations for names of rock-forming minerals. Am Mineral 95:185–187. https://doi.org/10.2138/am.2010.3371

Williams ML, Grambling JA (1990) Manganese, ferric iron, and the equilibrium between garnet and biotite. Am Mineral 75:886–908

Wilson AD (1955) A new method for the determination of ferrous iron in rocks and minerals. Bull Geol Surv Gt Britain 9:56–58

Wilson AD (1960) The micro-determination of ferrous iron in silicate minerals by a volumetric and a colorimetric method. Analyst 85:823–827

Wones DR, Eugster HP (1965) Stability of biotite: experiment, theory, and application. Am Mineral 50:1228–1272

Wynne-Edwards HR, Hay PW (1963) Coexisting cordierite and garnet in regionally metamorphosed rocks from the Westport Area, Ontario. Can Mineral 7:453–478

Yardley BWD (1977) Relationships between the chemical and modal compositions of metapelites from Connemara, Ireland. Lithos 10:235–242. https://doi.org/10.1016/0024-4937(77)90050-0

Zane A, Weiss Z (1998) A procedure for classifying rock-forming chlorites based on microprobe data. Rend Lincei 56:51–56. https://doi.org/10.1007/BF02904455

Zen EA (1981) Metamorphic mineral assemblages of slightly calcic pelitic rocks in and around the Taconic allochthon, southwestern Massachusetts and adjacent Connecticut and New York. US Geol Surv Prof Pap 1113. https://doi.org/10.3133/pp1113